PHILOSOPHICAL TRANSACTIONS OF THE ROYAL SOCIETY A MATHEMATICAL, PHYSICAL & ENGINEERING SCIENCES

Satellite Image Analysis Techniques Applied to Oceanography [and Discussion]

P. E. La Violette and J.-P. A. L. Muller

Phil. Trans. R. Soc. Lond. A 1988 **324**, 325-346
doi: 10.1098/rsta.1988.0023

Phil. Trans. R. Soc. Lond. A **324**, 325–346 (1987)
Printed in Great Britain

Satellite image analysis techniques applied to oceanography

By P. E. La Violette

Naval Ocean Research and Development Activity, NSTL, Bay St. Louis, Mississippi 39529-5004, *U.S.A.*

[Plates 1 and 2]

Infrared and visible spectral sensors on spacecraft can provide imagery of ocean conditions equivalent to a global network of *in situ* sensors. Oceanographers can now view all the world's oceans during one day's travel of a polar-orbiting satellite. The surface areas of complex ocean regions that have strong thermal and chemical gradients, such as the Gulf Stream in the Atlantic and the Kuroshio in the Pacific, are displayed in minute detail in the imagery provided by satellite infrared and visible sensors.

Because of the vast quantities of data involved in satellite infrared and visible imagery, computer techniques must be used to derive oceanographic information. A variety of basic computer image analysis techniques are required to do so. These basic techniques include selective enhancement, geographic registration, absolute ocean radiation and multiple-image composition. Through the use of these techniques, satellite and conventional oceanographic data can be integrated to form synergistically a powerful analytical tool for modern ocean research.

Introduction: general concepts

Although seemingly uniform to the uninitiated, the oceans of the world are highly variable; any given region has unique distinguishing physical characteristics. These characteristics are controlled by specific factors: the atmosphere, the seasonal migration of the Sun, the restriction of bottom topography, and the influx of thermally–chemically different waters from outside the region. Because these factors vary globally, the resulting characteristics of the ocean vary from region to region.

Many variations can be detected in infrared and visible satellite imagery. How this detection can be done with computer image analysis techniques is demonstrated in figures 1 and 2, plates 1 and 2. But before discussing these techniques, certain basic concepts must be understood.

The first and most important concept involves understanding the physics and the limitations of infrared and visible satellite data. For example, because of their altitude, satellites obviously have no direct contact with the ocean. Their instruments are restricted to sensors that detect the ocean's reflected or emitted electromagnetic radiation (figure 3). Since the atmosphere lies between the ocean and the satellite, the data received by the satellite are actually a summation of both the atmospheric and the oceanic signals. The emanations of the two régimes must be separated to derive quantitative oceanographic data. This separation, which will be demonstrated, can be difficult and requires the application of a second concept.

The second concept (and the main purpose of this paper) recognizes that satellite imagery produces vast amounts of data and that computer analysis techniques are required to

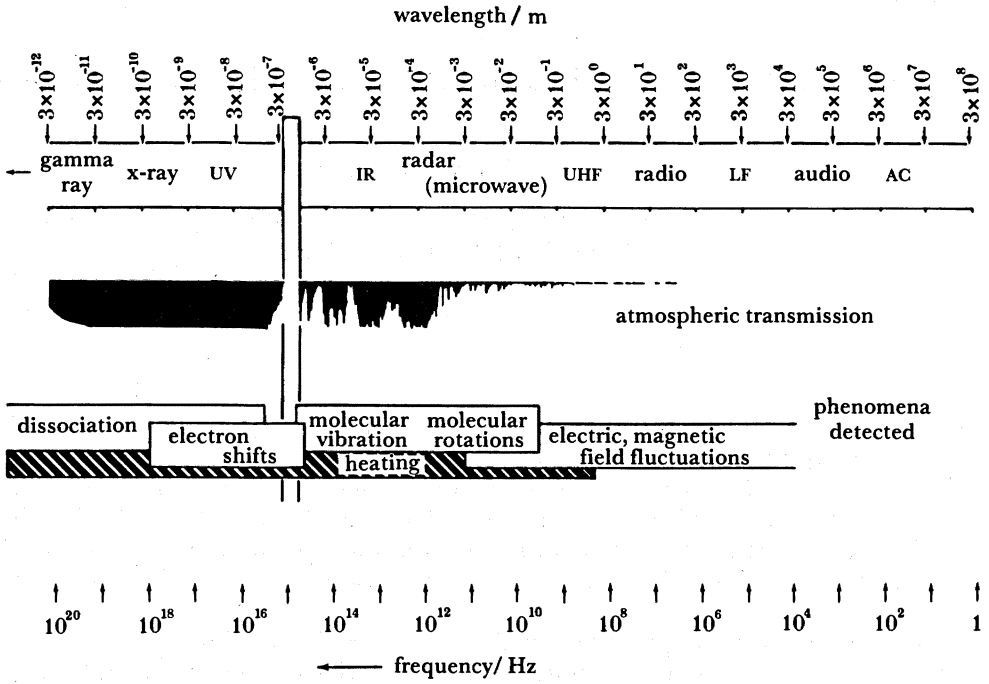

FIGURE 3. Characteristics of the electromagnetic spectrum significant to remote sensing of the ocean.

manipulate these data into usable form. Such techniques can be applied to satellite data by using small computers that interface with image processing and display hardware. These systems are available commercially and are relatively inexpensive. They are a prerequisite for any institution wishing to include satellite image processing as part of its oceanographic programme.

Various computer image analysis techniques can be applied to the study of a particular ocean region. However, in almost all selections, a basic set of techniques should be included: selective enhancement, geographic registration, absolute ocean radiation, and multiple-image composition. These basic techniques will be stressed here. As our skills and knowledge increase, these techniques will improve and, undoubtedly, new techniques will develop.

A final and very important concept is that the satellite data alone are not a panacea for studying the oceans. Satellite data are useful in that alone or in combination with other data

DESCRIPTION OF PLATE 1

FIGURE 1. (*a*) This cloud-free *NOAA*-7 AVHRR IR (channel 4, i.e. 10.3–11.3 μm) image of the eastern seaboard of the United States was taken on 28 April 1983. The registered, calibrated image shows the thermal convolutions of the Gulf Stream as it forms a border between the warmer waters of the Sargasso Sea and the coastal cold slope waters off the continental shelf (the darker portions of the picture are the warmer radiated temperatures of the scene).

The image shows the development of Gulf Stream meanders and cold- and warm-core eddies (rings) that were generated when the meanders pinched off. The warm-core ring at 67 °W is easily distinguished as being warmer than the older one northeast of Norfolk, Virginia. This westernmost ring entrained cooler slope water during its journey to this position and now has a cooler centre at the surface with warmer water on the edges. Other features are readily evident. Note the dark regions in the southern area that developed as a result of daytime heating. (Photograph courtesy of Jeffrey Hawkins, NORDA.) (*b*) Note that the details in the cold-water area northwest of the Gulf Stream in figure 1*a* are difficult to discern. In this enhancement the grey tones are set to display that region with the result that the area southeast of the Gulf Stream is poorly defined.

PHILOSOPHICAL TRANSACTIONS OF THE ROYAL SOCIETY A MATHEMATICAL, PHYSICAL & ENGINEERING SCIENCES

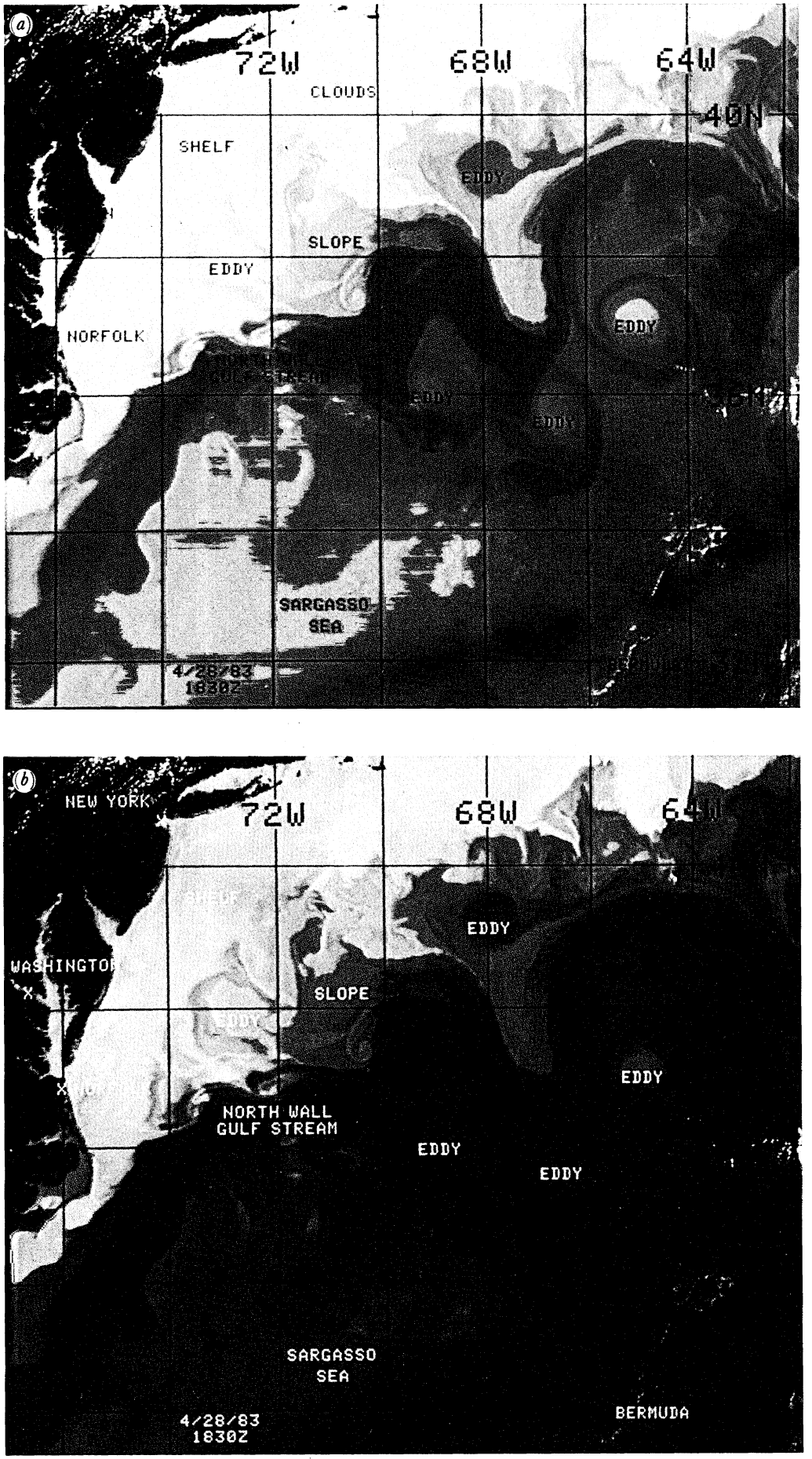

FIGURE 1*a*, *b*. For description see opposite.

PHILOSOPHICAL TRANSACTIONS OF THE ROYAL SOCIETY A MATHEMATICAL, PHYSICAL & ENGINEERING SCIENCES

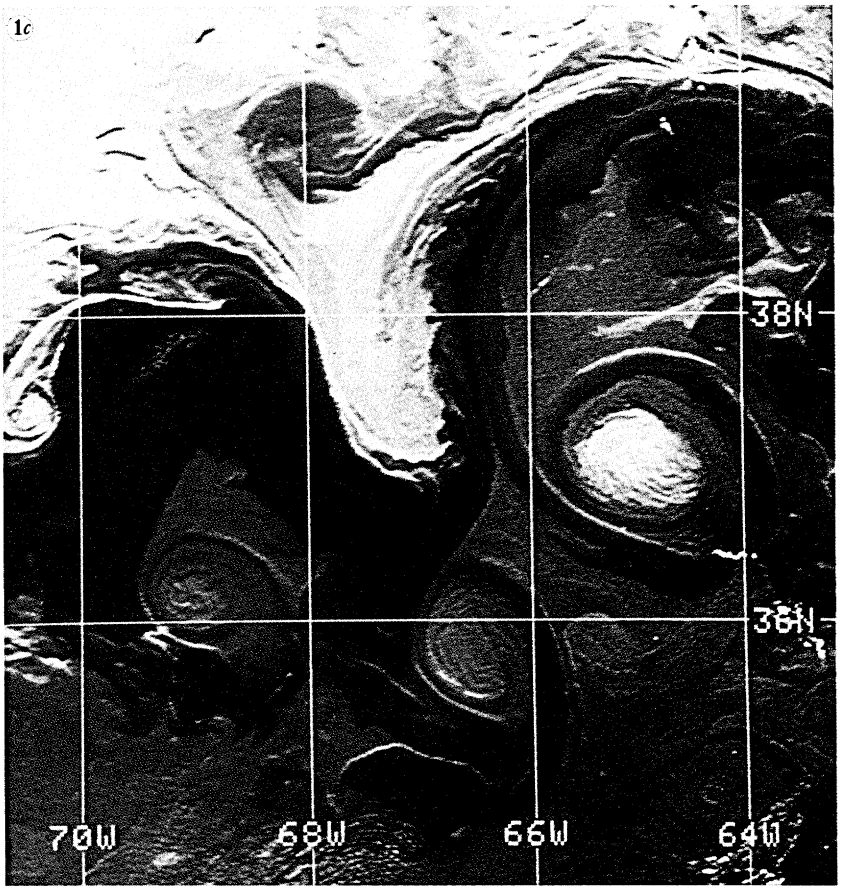

FIGURE 1*c*. For description see opposite plate 1.

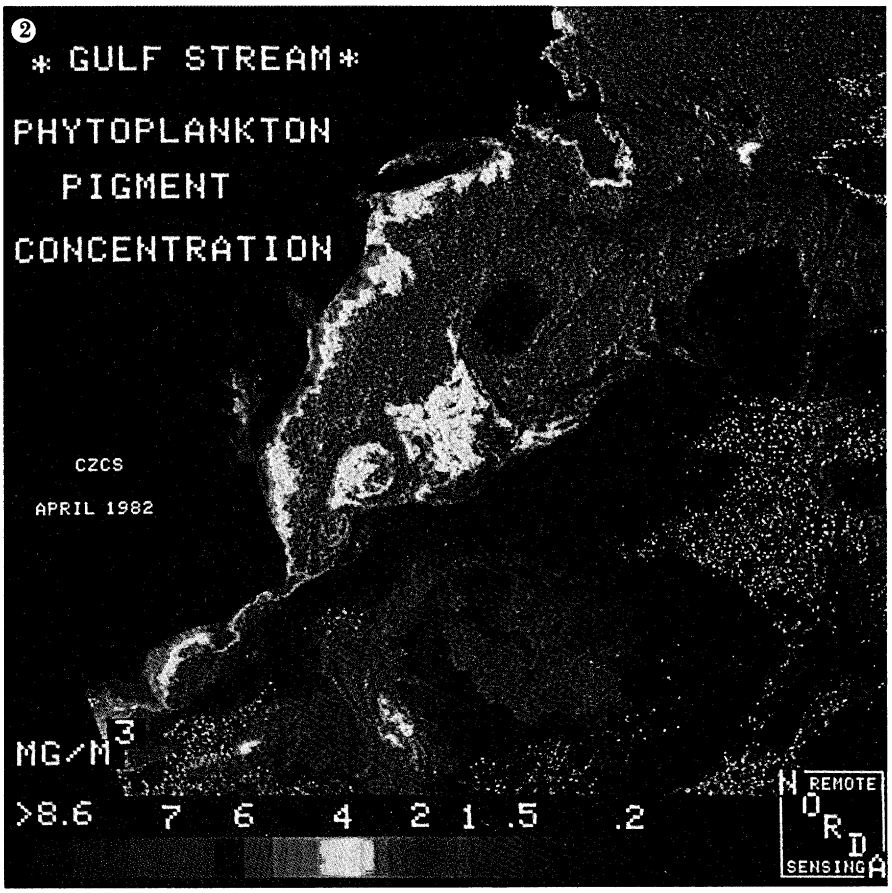

FIGURE 2. For description see opposite.

PHILOSOPHICAL TRANSACTIONS OF THE ROYAL SOCIETY A MATHEMATICAL, PHYSICAL & ENGINEERING SCIENCES

bases their main output is information. The intuitive skill of the ocean investigator will determine how well the data provide that information. In using satellite data, one must ask certain relevant questions. What created the surface effects seen in the imagery? How deep do these surface effects go? How do these surface effects relate to the characteristics of the deeper water? What conditions are normal? What conditions are abnormal?

In keeping with these concepts, the following sections discuss the physics and the limitations of infrared and visible satellite data, the computer analysis techniques needed to exploit these data, and examples of combined satellite and conventional oceanographic data analyses of two ocean regions.

Infrared and visible satellite data

Infrared satellite data

Infrared satellite data can be used to provide the radiometric surface temperature of the ocean. Ignoring atmospheric effects for the moment, observations in selected spectral ranges can be used to measure the equivalent blackbody temperatures of the ocean surface. In ocean regions where wind speeds are greater than 10 kn†, these temperatures are closely related to what oceanographers consider to be ocean surface temperature (i.e. the temperature of the approximate first metre of water).

Obtaining the oceans' surface temperatures from the altitude of a satellite presents a number of problems, however, and an understanding of these problems is necessary before the data can be used in ocean studies. The following notations are adapted from Holter (1970).

Planck's fundamental radiation equation gives the spectral distribution of radiation from a self-emitting perfect radiator (blackbody) with uniform temperature ($W_{B\lambda}$). Planck's law applies to the entire electromagnetic spectrum and can be expressed in terms of spectral radiant emittance as

$$W_{B\lambda} = C_1 \lambda^{-5} [\exp(C_2/\lambda T) - 1]^{-1}, \quad (1)$$

where C_1 and C_2 are radiation constants, λ is the wavelength, and T is the temperature of the radiating surface. The units of the equation are 10^{-7} J cm^{-2} s^{-1} μm^{-1}.

† 1 kn = 1.852 km h^{-1} $\approx$ 0.514

Description of plate 2

Figure 1. (*c*) This higher resolution (1 km) subsection of figure 1*a* was processed with a modified Frei-Chen edge enhancement filter. Filter weights were chosen so that the intensity at each point was replaced by a 3 × 3 finite difference approximation to the original image. Linear contrast enhancement was applied to the image before the filtering. The results show the impression of relief based on the sea surface temperatures. The relief is the opposite of reality in that the white (cold-core) rings should represent a depression in the ocean surface and not a rise. (Photograph courtesy of Matthew Lybanon, NORDA.)

Figure 2. This *Nimbus* 7 czcs false-colour image of the same ocean area as figure 1 was taken on 24 April 1982. In this instance, the registered, calibrated image has been atmospherically corrected and presents colour variations representing values that result from ratioing the czcs 450 and 550 spectral channels. Although the values derived from this ratio are normally used to show the chlorophyll distribution in the ocean, here they are equally instructive in showing the region's current and frontal distribution. Note that the temperature values presented as grey tones in figures 1*a*, *b* could also have been displayed in colour in the way shown here. The advantage of colour goes beyond aesthetics in that the colour scale can show a greater range than the black and white scale. A case in point is that the details of the ocean features northwest of the Gulf Stream are clearly shown in this figure, whereas they had to be added as a subimage in figure 1. (Photograph courtesy of Robert A. Arnone, NORDA.)

In Nature, of course, most objects are not perfect radiators. The radiative efficiency factor, ϵ, or spectral emissivity, of these imperfect radiators (greybodies) varies with wavelength and may be defined as

$$\epsilon_\lambda = W_\lambda / W_{\mathrm{B}\lambda}, \tag{2}$$

where W_λ is the spectral radiant emittance of a greybody for a given wavelength. The spectral emissivity of different objects may range from close to zero for poor radiators to unity for perfect radiators.

Such greybodies as the ocean approach being blackbodies within selected spectral bands. The important issue in most cases, therefore, is the characteristic emissivity for the specific band being monitored. Equations (1) and (2) can be used to obtain the spectral radiant emittance of any surface of known temperature and spectral emissivity.

The surfaces of greybodies reflect, as well as emit energy. Kirchhoff's law states that if a surface is optically opaque, then the spectral reflectivity, ρ_λ, and the spectral emissivity, ϵ_λ, of the surface have the relation

$$\rho_\lambda = 1 - \epsilon_\lambda. \tag{3}$$

From this relation we know that infrared radiation from a surface is the result of a combination of self-emission of the surface and the reflection of a portion of the incident radiation on that surface.

If we apply these principles to the oceans, the infrared radiation emitting from the ocean surface comes from (*a*) the self-emission of the topmost radiating molecule of water and (*b*) the reflection of portions of energy incident from such atmospheric sources as clouds, water vapour, carbon dioxide and aerosols. The sum of these two radiation components can be defined as the effective spectral radiance emittance of the ocean surface, $W_{\mathrm{e}\lambda}$:

$$W_{\mathrm{e}\lambda} = \epsilon_\lambda W_{\mathrm{B}\lambda} + \rho_\lambda W_{\mathrm{a}\lambda}, \tag{4}$$

where the self-emission component is $\epsilon_\lambda W_{\mathrm{B}\lambda}$ and the surface reflection component is $\rho_\lambda W_{\mathrm{a}\lambda}$.

Where the effective spectral radiance of the sea surface is measured from satellite altitudes, the additional effect of infrared absorption and emission by atmospheric constituents (chiefly, gas molecules of water vapour, carbon dioxide, nitrogen and ozone) must be considered. At these altitudes, N, the upward spectral radiance at a given zenith angle, θ, and wavelength, λ, is given by

$$N_\lambda(\theta) = W_{\mathrm{e}\lambda}(T_{\mathrm{s}})\,\tau_{\lambda\mathrm{a}}(\theta) + \int^{\text{(atmosphere)}}_{\text{(ocean)}} W_{\mathrm{a}\lambda}(T_{\mathrm{a}})\,\mathrm{d}\tau_\lambda(\theta), \tag{5}$$

where $W_{\mathrm{e}\lambda}$ is the effective spectral radiant emittance at temperature T_{s}, $\tau_{\lambda\mathrm{a}}$ is the spectral transmissivity through the atmosphere, τ_λ is the spectral transmissivity through a layer that extends from a given altitude to the top of the atmosphere, and $W_{\mathrm{a}\lambda}$ is the spectral radiant emittance of the atmosphere at temperature T_{a}.

The first term on the right of (5) is the radiant emittance of the ocean surface to space; the second term is the emittance of a cloud-free atmosphere, integrated from the ocean surface to the top of the atmosphere.

Molecular absorption by atmospheric gases is important at infrared wavelengths. As mentioned, the important absorbing gases in the infrared are water vapour, carbon dioxide, nitrogen and ozone. In those spectral ranges where one or more of these gases are strongly

absorbent, the atmosphere for all practical purposes is opaque. Conversely, in some regions, the absorption by these gases is weak.

It is these latter regions, or atmospheric 'windows', that must be used to measure the ocean's effective spectral radiation (figure 3). The boundaries of these windows are difficult to define because the transmissivity of the atmosphere depends on the concentrations of the active absorbing gases present (thus, the distance the radiation must travel through the atmosphere becomes a factor, because a low-angle look at an ocean region would pass through a thicker atmosphere and, hence, larger amounts of absorbing gases).

The amount of energy radiated by a blackbody surface is given by Planck's function. From (1) and figure 3, it can be seen that the 8–12.5 μm window regions have the maximum emitted energy at temperatures near 300 K. This range, then, is the most effective for oceanographic use and the one most used by passive ocean thermal sensors. In the 3.4–4.2 μm window, reflected sunlight and emitted radiation are almost equal in terms of energy. Thus, during daylight hours, data in this spectral range are contaminated by reflected sunlight.

Visible satellite data

In the visible portion of the spectrum (0.4–0.8 μm), the main signal-generating mechanism from the ocean is the backscatter of incident sunlight (the other source is comparatively minor: the fluorescence of marine microorganisms). Visible remote sensing is limited to day periods and regions where the Sun is at least 30° above the horizon. The ocean's ambient light is reflected into space in many ways, some of which include Fresnel reflection from the surface, diffuse scattering by surface foam, and scattering and absorption within the water column.

Fresnel reflectance tells us nothing directly about the biological–chemical constituents within the ocean. Where such specular reflection (or sun glint) occurs, the effect is generally so severe that no subsurface colour information can be retrieved. (However, sun-glint photographs of roughness patterns in the ocean surface have been qualitatively used to provide information on ocean circulation in much the same manner as imagery from synthetic and real aperture radars. Although these photographic data show great potential, they have not been practically adapted to image processing and, thus, are beyond the scope of this paper.)

The upwelled spectral radiance (or colour) of the ocean results from the backscatter of light energy from below the surface (less the spectral absorption). Measurements of upwelled radiance can provide information on the ocean's biological production and optical properties, and can act as tracers or descriptors of physical ocean events.

There is a practical depth limit from which the radiance is reflected. Gordon & McCluny (1975) call the depth at which the spectral radiance downwelled from the surface falls to 1/e of its initial energy 'the first optical attenuation length'. Approximately 90% of the upwelled radiance is backscattered before this depth, and radiance from greater depths is negligible. For practical purposes, then, the upwelling spectral radiance of the ocean measured at the water surface may be considered to be the integration of the radiant backscatter and the spectral absorption within the first optical attenuation length.

For clear ocean waters, the attenuation length is normally 20 m or greater; in coastal areas, the attenuation length is typically 2–4 m. An inverse relation of the attenuation length – the diffuse attenuation coefficient, k – is normally used as a measurement of ocean radiance. Although k depends on the vertical distribution of scattering and absorption properties, it does not reveal the actual depth at which the optical variability occurs. In other words, it is possible

PHILOSOPHICAL TRANSACTIONS OF THE ROYAL SOCIETY A MATHEMATICAL, PHYSICAL & ENGINEERING SCIENCES

to have the same water-leaving radiance at the surface for two separate areas whose optical properties are vertically very different. A relatively turbid, homogeneous water mass can display similar surface radiance to a clear water mass with a thin, turbid layer lying within the attenuation depth. Thus, any vertical variation in the optical properties that occurs in the first attenuation length can significantly influence the upwelling water-leaving radiation sensed by an ocean colour scanner.

The concentrations of phytoplankton pigments are largely responsible for the ocean's optical properties (these pigments are largely representative of chlorophyll-a and also include the phaeopigment concentration (Gordon *et al.* 1983). The spectral absorption ability of the pigment significantly affects upwelling radiance (Arnone & La Violette 1986). The strong correlation between this biological pigment and the water optical properties provides an excellent measurement of a region's productivity.

Atmospheric effects are also significant when sensing the ocean from space at visible wavelengths. As much as 90% of the radiance detected at satellite altitudes can be expected to be due to atmospheric scattering (Gordon 1978). Atmospheric scattering arises from scattering from gas molecules (called Rayleigh scattering) and from aerosols or particulates (called Mie scattering). The molecular composition of the atmosphere is relatively constant so that the removal of the Rayleigh component of the earth's radiance is not too complex. However, the aerosol effects, depending on particle concentration, composition and size distribution, are highly variable both spatially and temporally.

Limitations of infrared and visible satellite imagery

Most of the infrared and visible satellite imagery that can be used to define oceanographic events has limitations imposed by the blockage of clouds or by the integration of the ocean signal with the intervening atmospheric moisture and aerosols. Many methods have been formulated to minimize these effects; several will be discussed.

A second important limitation of infrared and visible satellite imagery is that these data represent the surface layers of the ocean. In the case of infrared imagery, the restriction is more severe because these data represent the 'skin' radiation of the ocean. In ocean regions that undergo extremely calm conditions and high solar radiation, the infrared imagery display abnormally high temperature readings, which are representative of extremely shallow surface heating rather than the temperature of the first metre of the water column (cf. the southern area of figure 1*a*). When this type of heating occurs, it is best to use night imagery of the region; at night solar heating is not present to create stratified conditions, and the shallow stratified layers left from the day are destroyed by dynamic mixing due to the ocean's normal thermal radiation. Most of the visible range imagery represents near-surface radiation (i.e. the portions of a visible image that shows upwelled radiance, not Fresnel reflection), so these data can be used to display frontal boundaries instead of the thermal imagery when shallow surface heating is a problem (cf. figure 2) and night-time infrared imagery is not applicable.

The satellites

Four satellite series now provide infrared and visible oceanographic data: *GOES* and *Meteosat* (in geosynchronous orbits), and NOAA and *Nimbus* (in polar orbit). Because the resolution of the *GOES* and *Meteosat* data is poor when compared to that of the NOAA and *Nimbus* data, this discussion will be limited to data from the latter.

PHILOSOPHICAL TRANSACTIONS OF THE ROYAL SOCIETY A MATHEMATICAL, PHYSICAL & ENGINEERING SCIENCES

The NOAA satellite series are operational satellites that normally carry the same sensor suite on each new spacecraft. Thus, image-analysis techniques useful for a specific sensor aboard the NOAA series can be used on data from almost any satellite in the series.

The NOAA advanced very high resolution radiometer (AVHRR) is a good example of an oceanographically useful sensor that has been aboard all NOAA satellites since *TIROS-N* (i.e. all NOAA satellites after *NOAA*-4). As the NOAA satellites are placed in Sun-synchronous orbits (figure 4), the AVHRR aboard each satellite can repeatedly detect the thermal (AVHRR IR)

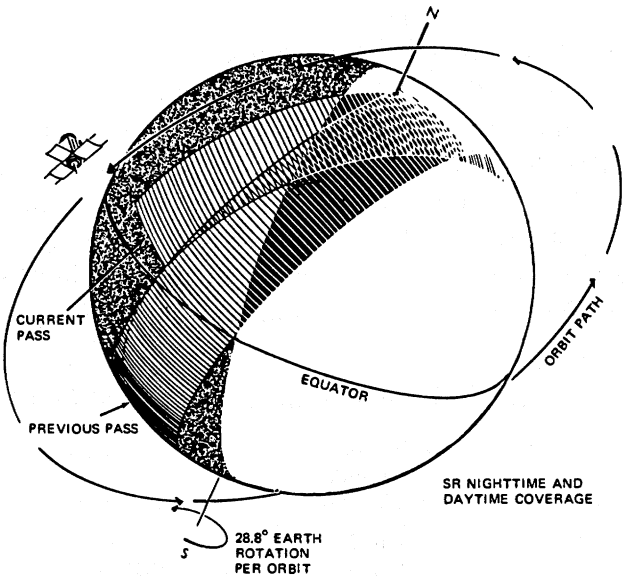

FIGURE 4. The Sun-synchronous, polar orbit of the NOAA satellite. Note the increase in the overlap of successive orbits near the poles.

and visible (AVHRR V) emissions of any region of the Earth at least twice each day. Thus, for cloud-free regions of the globe, 10-bit data from the AVHRR IR can convey descriptions of the surface thermal structure of the world's oceans approximately every 12 hours. A resolution of about 1 km and an absolute accuracy of ± 0.3 °C are obtained. Detailed information on the NOAA satellites and the AVHRR can be found in Schwalb (1978) and Hussey (1979).

Figure 1 is an example of the thermal gradient display made possible by using *NOAA*-7 AVHRR IR data. In this thermal image the equivalent notation of grey shades to temperature variation is the standard method used in satellite oceanography; i.e. higher temperatures are displayed as increasingly dark tones and lower temperatures as lighter tones, and the whitest feature is usually the cold tops of clouds. In most of the imagery presented here, a step function is used to display clouds as black. This highly useful display function de-emphasizes the seeming omnipresence of white clouds in an image, while allowing the presentation of sometimes subtle ocean thermal features.

For long-term operational purposes, the *Nimbus* research satellites are the least usable of the polar orbiters because the sensors on these satellites are usually one-time affairs; each new *Nimbus* spacecraft has a different suite of experimental sensors. The *Nimbus*-7 coastal zone colour scanner (CZCS), which can directly detect the variation and distribution of the ocean's chemical and biological material, is a good example. As figure 2 shows, however, the CZCS can indirectly provide information on currents and frontal features in the water.

Although the czcs has proven to be a highly successful oceanographic sensor, it is not scheduled to be placed on any of the upcoming *Nimbus* spacecraft. Much of what will be said here, however, is applicable to other visible range sensors and provides good examples to follow when using similar sensors in the future.

The 8-bit data from the *Nimbus*-7 czcs can detect subtle ocean colour changes by using five visible spectral bands selected for their ocean-viewing qualities (unlike *Landsat*, whose visible spectral bands are highly useful for land viewing but poor for looking at the oceans). These five channels are centred at 0.443, 0.520, 0.670, 0.750, and 1.150 μm, and have a resolution at nadir of 800 m. The first four channels are in the visible and the fifth is in the near infrared (reflective).

The polar orbits of the *Nimbus* satellites are not Sun-synchronous as are the NOAA satellites. Rather than passing over the earth at the same time each day, the orbit is such that a given region at 40° north or south is viewed on approximately three out of four days at around local noon. A description of the *Nimbus*-7 satellite and czcs can be found in Hovis *et al.* (1980).

It is important to note that because they are polar orbiters, both NOAA and *Nimbus* provide far more coverage in the polar regions than nearer the equator (cf. figure 4 and table 1). This coverage can give a tremendous advantage in studying the oceans in these remote regions and allows such extremely useful techniques as multi-image compositing.

TABLE 1. *TIROS-N* ORBIT PREDICTIONS FOR OSLO, 30 OCTOBER 1980

pass	time of maximum elevation (Z)	time interval
1	02h27	—
2	04h08	01h41
3	05h29	01h41
4	10h45	06h16
5	12h24	01h39
6	15h46	03h22

SATELLITE IMAGE ANALYSIS TECHNIQUES

Basic computer techniques

Four basic image analysis techniques should be used to derive oceanographic information from satellite imagery: selective enhancement, geographic registration, absolute ocean radiation and multiple-image composition. Any number of subsets and combinations of these techniques are possible, such as edge enhancement or the ability to make loop movies of selected series of registered images.

Selective enhancements

Selective enhancement is one of the simplest and most useful tools of satellite image analysis techniques. Although the grey-scale wedge in the imagery is limited to a finite number of grey bands, these bands can be assigned to display selected ocean phenomena in the manner shown in figures 1*a*, *b* and 5*a*. Another method to emphasize the image's oceanic information utilizes edge enhancement, as shown in figure 1*c*. Colour wedges, as used in figure 2, can be used instead of the grey wedge. When the image is registered to a standard projection and the grey (or colour) shading is equivalent to absolute temperature or bio-optical values, the enhancement technique can be quantitatively, as well as qualitatively, useful.

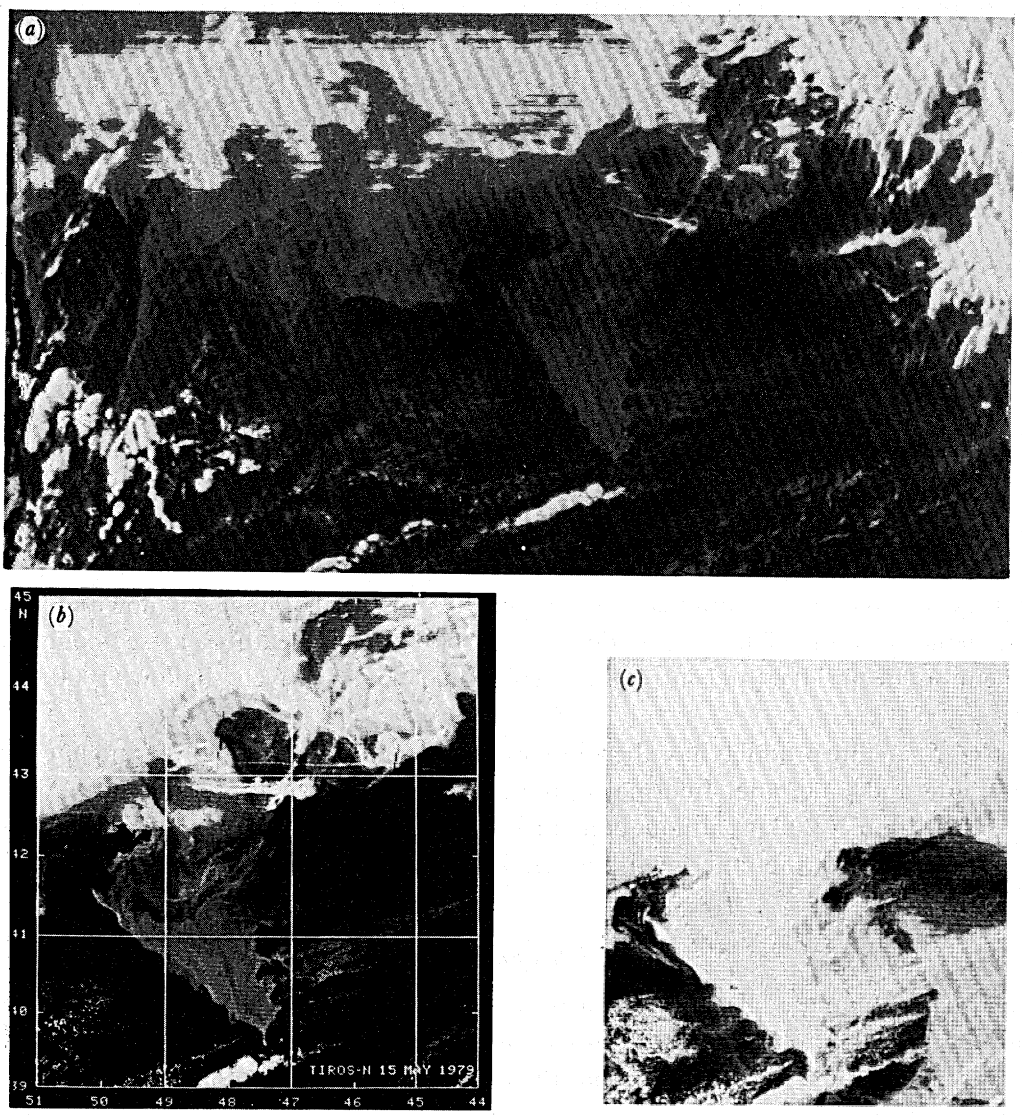

FIGURE 5. (*a*) Standard *TIROS-N* infrared (10.5–11.5 μm) image product from NOAA/NESDIS for 15 May 1979 showing the meandering pattern of the Gulf Stream southeast of Newfoundland, Canada. (*b*), (*c*) Two enhancements of Mercator-registered imagery of the 15 May 1979 *TIROS-N* infrared image shown in (*a*) to show various aspects of a cohesive mass of cold water that extruded into the eastward path of the Gulf Stream. Details of the cold-water extrusion are shown in (*b*), and details of the northward movement of warm water (Gulf Stream) into the eastern section of the area are shown in (*c*) (Holyer *et al.* 1980).

Geographic registration

Finding the accurate geographic location of ocean features seen in a satellite image is an important input to oceanographic analysis of the image, especially if the feature is to be correlated with data from other satellites, ships, or aircraft. Correlation is possible by using NOAA satellite data distributed in computer compatible tapes (CCT) by satellite data distribution centres, such as NOAA/NESDIS (U.S.) and CMS (France). These CCTs have geographic positions incorporated in a systematic fashion throughout the AVHRR data. Imagery constructed from these data has been shown to contain location accuracies with a standard deviation of 1.7 km about mean errors of 3.7 km (Clark & La Violette 1981).

The distribution of geographic locations in the AVHRR data allows an important image analysis technique to be used beyond geographically positioning a point on an image. It allows an image to be displayed in a standard map projection, such as Mercator or polar stereographic. Now, sets of NOAA imagery can be made that have a common projection and measurements made on temporal and spatial scales that were not easily done before. The method often used to warp NOAA-type data to various map projections uses two-dimensional, third-order polynomials derived from the latitude–longitude data on the CCT. This accuracy may be further improved if the ocean region has well-distributed landmarks. Almost all the imagery presented in this paper has been registered to a standard map projection. The exception is figure 5*a*, which shows how the unregistered image looks as received from the satellite, i.e. as a skewed cylindrical projection.

Figures 6 and 7 show thermal imagery of the Grand Banks and the Alboran Sea warped to Mercator projections. The warping was done with sufficient accuracy (± 1.0 km) to allow the overlay of data from other satellites, aircraft, and ships. For figure 7, the successive imagery was used to produce a time-lapse sequence, or cine loop, of ocean features with no noticeable misregistration jitter. The frames shown in figure 7 were a portion of a movie covering a period of ten days. The overlay of isobaths on registered NOAA thermal imagery shown in figure 8 is a good demonstration of how such deep-ocean bathymetric features as seamounts and a prominent but deep ridge can control the circulation of comparatively shallow (1000 m) ocean features.

The *GOES* satellite products have benchmark records that associate sample and line numbers with latitude and longitude. Informal evaluation has found these products to be generally accurate to within ± 20 km, although errors of several hundred kilometres are possible. The positional accuracy of the other environmental satellites has not been evaluated.

Absolute ocean radiation

If the quantitative use of satellite data is to be expanded, an accurate measurement of the absolute ocean radiation is needed. This measurement requires, first, the radiometric calibration of the satellite sensor and, second, the removal of the portion of the signal that results from the atmosphere.

Continuous radiometric calibration of the NOAA AVHRR IR channels is done on-board the satellite. Assuming the output of the thermal detector is linear with input energy, a calibration curve is established by using only two points. One point is the scanner view of deep space (zero radiance), and the other point is the view of the scanner housing (290 K). Four platinum resistance thermistors, whose outputs are included in the data stream of each scan line, monitor the exact temperature of the housing. These data are averaged over several sweeps of the sensor mirror and are then transmitted with the terrestrial radiation data to the ground station. The resultant curve provides a dynamic calibration that is used to track and compensate for any drift in the performance of the detector and associated electronics. CCTs received from central satellite data collection stations, such as NOAA/NESDIS, normally contain these calibration data.

The oceanic signal lost due to the overriding signal of the atmosphere places a strong limitation on the oceanographic use of infrared and visible imagery. With infrared imagery, this problem is especially prevalent in data taken at mid- and low latitudes in summer.

PHILOSOPHICAL TRANSACTIONS OF THE ROYAL SOCIETY A MATHEMATICAL, PHYSICAL & ENGINEERING SCIENCES

FIGURE 6. Mercator-registered *TIROS-N* infrared (10.5–11.5 μm) imagery of the waters of the Grand Banks southeast of Newfoundland, Canada, for four successive days in May 1979 (the series includes the image in figure 5). The imagery shows the movement of frontal shear waves moving along the boundaries of a cohesive mass of cold water that had been extruded into the eastward path of the Gulf Stream. The shear waves were active on both the western and eastern fronts of the cold-water mass and moved at phase speeds of approximately 70 cm s^{-1}, a period of approximately 0.83 days and a wavelength of 50 km. Movement during a period of 12 hours is marked by arrows. A comparison of these derived phase speeds with *in situ* measured current speeds shows the waves were moving at nearly the same speed as the cold-water currents. The imagery shows that rapid movement within the ridge feature was also measurable. Tracking the displacement of several cold filaments within the cold water over several days shows they averaged 70 cm s^{-1}. These displacements are similar to velocities measured by satellite drifter buoys tracked during the same period. The imagery has not been atmospherically corrected (La Violette 1983).

Of several possible solutions, the most popular is the multichannel single-satellite approach (McClain *et al.* 1977).

The NOAA AVHRR IR has three channels centred at the 3.7, 11 and 12 μm atmospheric windows. The spectral bands thus have relatively high transmittances with regard to middle- and far-infrared spectral range energy emitted by the ocean surface. As mentioned earlier, the most significant atmospheric absorption constituents in these regions are water vapour and aerosols. However, the amount of absorption varies for each spectral region. The 3.7 μm channel has a transmittance of 90 %, the 11 μm channel has a transmittance of 75 %, and the

PHILOSOPHICAL TRANSACTIONS OF THE ROYAL SOCIETY A MATHEMATICAL, PHYSICAL & ENGINEERING SCIENCES

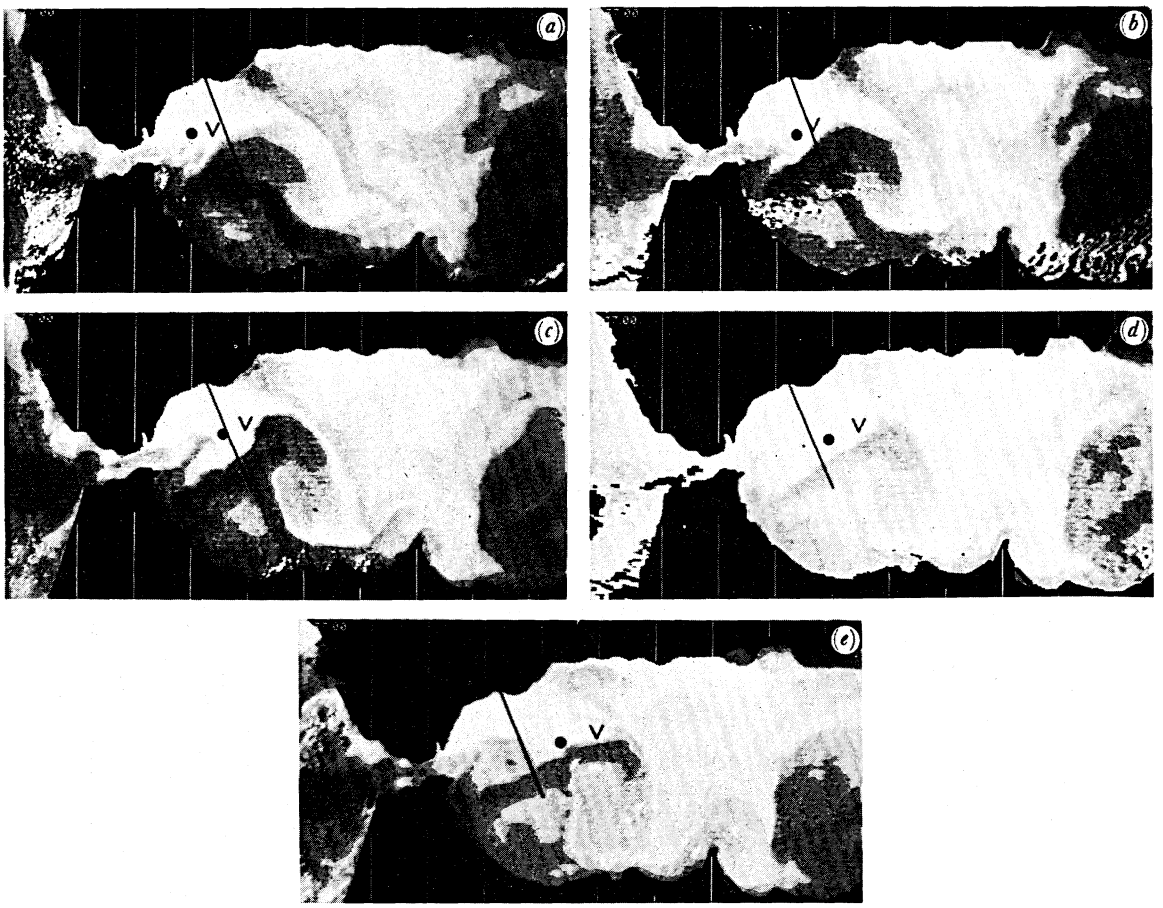

FIGURE 7. *NOAA*-7 AVHRR-IR imagery of the Alboran Sea collected as part of the Donde Va? experiment during October 1982. The dot and the 'V' in the images show the advection of two submesoscale cold features about the permanent gyre located in the Alboran Sea. The black line represents a line of current meter moorings positioned during the Donde Va? experiment. A close examination of the imagery shows that other unmarked features were also being advected and that their generation was probably tide related. Continuous monitoring of these cold-water features was possible because of the twice-daily (about every 12 h) spacing of the *NOAA*-7 overpasses. After registration to a Mercator projection (accuracy ± 1 km) and an atmospheric correction to arrive at absolute temperatures, analysis of the displacement of the cold features in successive images shows their apparent origin east of Gibraltar, their average speeds of 40 cm s^{-1} around the gyre, and their apparent entrailment into the incoming Atlantic water east of Gibraltar (La Violette 1984). (*a*) 14h32 GMT 6 October; (*b*) 02h56 GMT 7 October; (*c*) 14h22 GMT 7 October; (*d*) 02h44 GMT 8 October; (*e*) 14h08 GMT 8 October.

12 μm channel transmittance is 80%. (Although limited to night use, one of the preferred channels to use because of its high transmittance rate is the 3.7 μm channel; however, high noise levels in this channel in all of the post-*TIROS-N* AVHRR IRs have precluded any real use of a three-channel algorithm. Until now only a two-channel algorithm has been used.)

These variations in infrared transmittance for the same ocean scene are the basis of the multiple-channel algorithm. The algorithm uses a correlation made by subtracting the effects of one channel from another; the remainder is a function of the amount of moisture present in the atmosphere. The two-channel equation takes the form

$$\text{MCSST} = A_1(T_{11}) + A_2(T_{12}) + C,$$

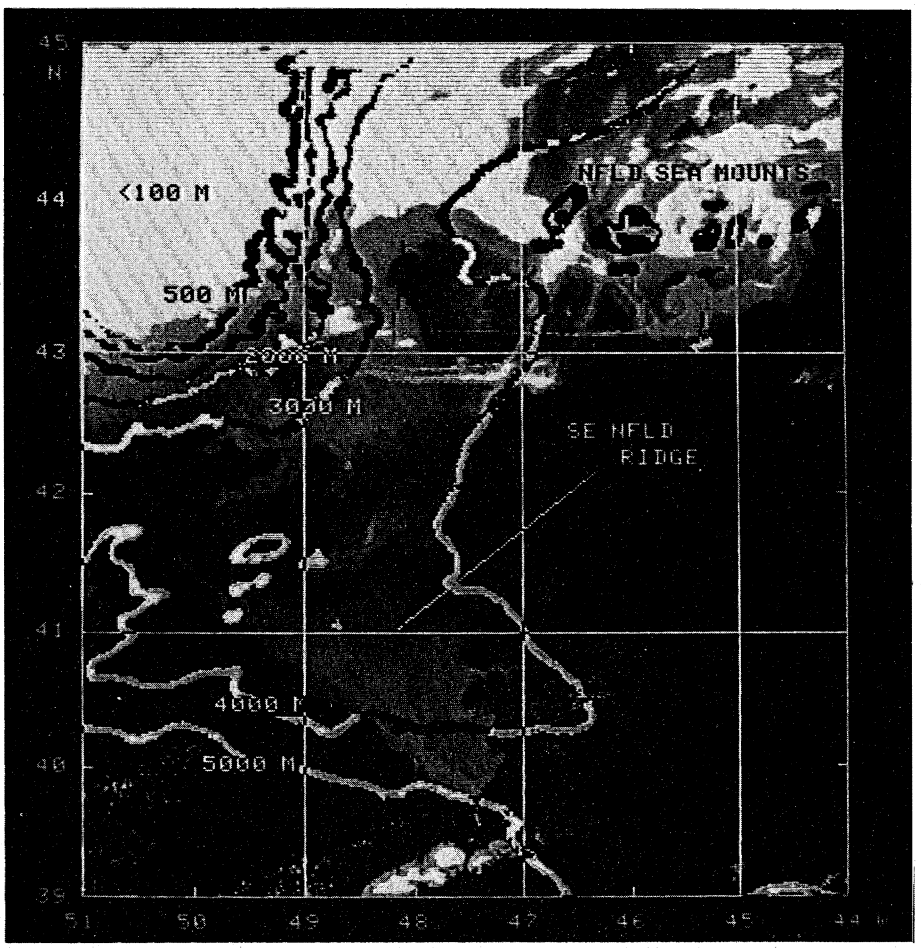

FIGURE 8. *TIROS-N* image for 15 May 1979 overlain with the 500, 1000, 2000, 3000, 4000, and 5000 m isobaths (Holyer *et al.* 1980).

where MCSST is the multichannel sea surface temperature, T_{11} is the measured radiative temperature in the 11 μm channel, T_{12} is the measured radiative temperature in the 12 μm channel, A_1, A_2 and C are coefficients derived from a best fit to empirical surface data.

If the greatest atmospheric problem with infrared data of the ocean is water vapour, with aerosols playing a minor role, then the reverse is true of visible range data. Aerosols are not only the major absorber–scatterer of the visible atmospheric signal, but their effect often results in a loss of almost 90% of the ocean signal.

The most widely accepted method for correcting the effects of aerosols in CZCS data requires extensive computer manipulation involving assumptions about the scattering properties of the local atmosphere and ocean. The method uses a mathematical atmospheric model based on single-scattering theory (Gordon & Clark 1980*a*)

$$L_{W(\lambda)} = L(\lambda) - L_{\mathrm{R}}(\lambda) - (F(\lambda)/F(670))\,(L(670) - L_{\mathrm{R}}(670)), \tag{7}$$

where $L_{W(\lambda)}$ is the upwelling radiance from the ocean at wavelength λ, $L(\lambda)$ is the radiance observed from space, $L_{\mathrm{R}}(\lambda)$ is the calculated Rayleigh scattering radiance of the atmosphere, $F(\lambda)$ is solar flux.

The Gordon & Clark (1980*a*, *b*) method assumes the czcs 0.670 μm channel can be used as a measure of the atmospheric aerosol concentration. Through a weighted subtraction of this channel with appropriate subtraction of Rayleigh scattering, the effective upwelling radiance from the ocean surface can be computed for the czcs 0.443, 0.520, and 0.550 μm channels.

However, several problems are associated with this correction method. The first problem involves the proper selection of the Ångström exponent. The Ångström exponent relates the wavelength-dependence of the aerosol optical thickness and single scattering albedo of the aerosols. (For a more complete explanation, see Gordon & Clark 1980*a*.) Gordon & Clark (1981) suggest that the radiance values of clear water in any czcs image be used to obtain this value. This technique, however, requires knowing the location of clear-water areas within the czcs image. Furthermore, the assumption is made that the Ångström coefficient over the clear water is the same throughout the image. If this assumption is not valid, the selected Ångström exponent value for one part of the image will produce erroneous values when applied to other portions of the image (Arnone 1983*a*, *b*).

To overcome this difficulty, Arnone & La Violette (1984) developed an interactive analysis procedure that defines the optimum coefficient for the entire image scene. This method was used for the czcs images presented in figures 2 and 11.

A second problem with the Gordon & Clark (1980*a*) correction procedure arises from the assumption that water has zero upwelling radiance at 0.670 μm. This assumption is logical for open ocean and shelf-type water masses where minimal concentration of suspended sediments occurs. However, significant upwelled radiance at 0.670 μm occurs in turbid coastal waters (Smith & Wilson 1981; Arnone 1983*a*, *b*). For these coastal areas, an underestimation of the absolute upwelling radiance in the correct czcs channels will result if this method is used.

Arnone & La Violette (1986) used the ratio of the absolute upwelling radiance for the 0.443 and 0.550 μm channels (i.e. 0.443/0.5500 to derive both the diffuse attenuation coefficient k at 0.490 μm (Austin & Petzold 1980) and the phytoplankton concentration (Gordon & Clark 1980*a*)). This method implies an inherent relation between k and phytoplankton concentration.

Multiple-image composition

The problem of clouds blocking the infrared satellite sensor's view of the ocean has long plagued oceanographers. Fortunately, ocean events change more slowly than atmospheric events. By using this fact as a basis, an analysis technique that minimizes cloud and atmospheric contamination can be arranged. This method composites the highest temperature values for a given region from infrared data collected over a period of several days (La Violette & Chabot 1969). The technique applies to any accurately registered thermal IR imagery using a common projection (figure 9).

One limitation of this method is that short-term effects are smeared in the final composite. Also, the composite is biased toward the period when the area was cloud-free. Like any such data restriction problems, these limitations can be taken into account and weighted according to the desired objective. Essentially, the user is faced with the problem of using the smallest number of satellite passes that will give the most cloud-free conditions and do the least smearing of ocean features.

The technique can be used most advantageously with ocean data from the higher latitudes. Here, the increased number of overflights each day by the polar-orbiting satellites allow composites to be made of several passes in a given day (table 1). As many of the storm systems

PHILOSOPHICAL TRANSACTIONS OF THE ROYAL SOCIETY A MATHEMATICAL, PHYSICAL & ENGINEERING SCIENCES

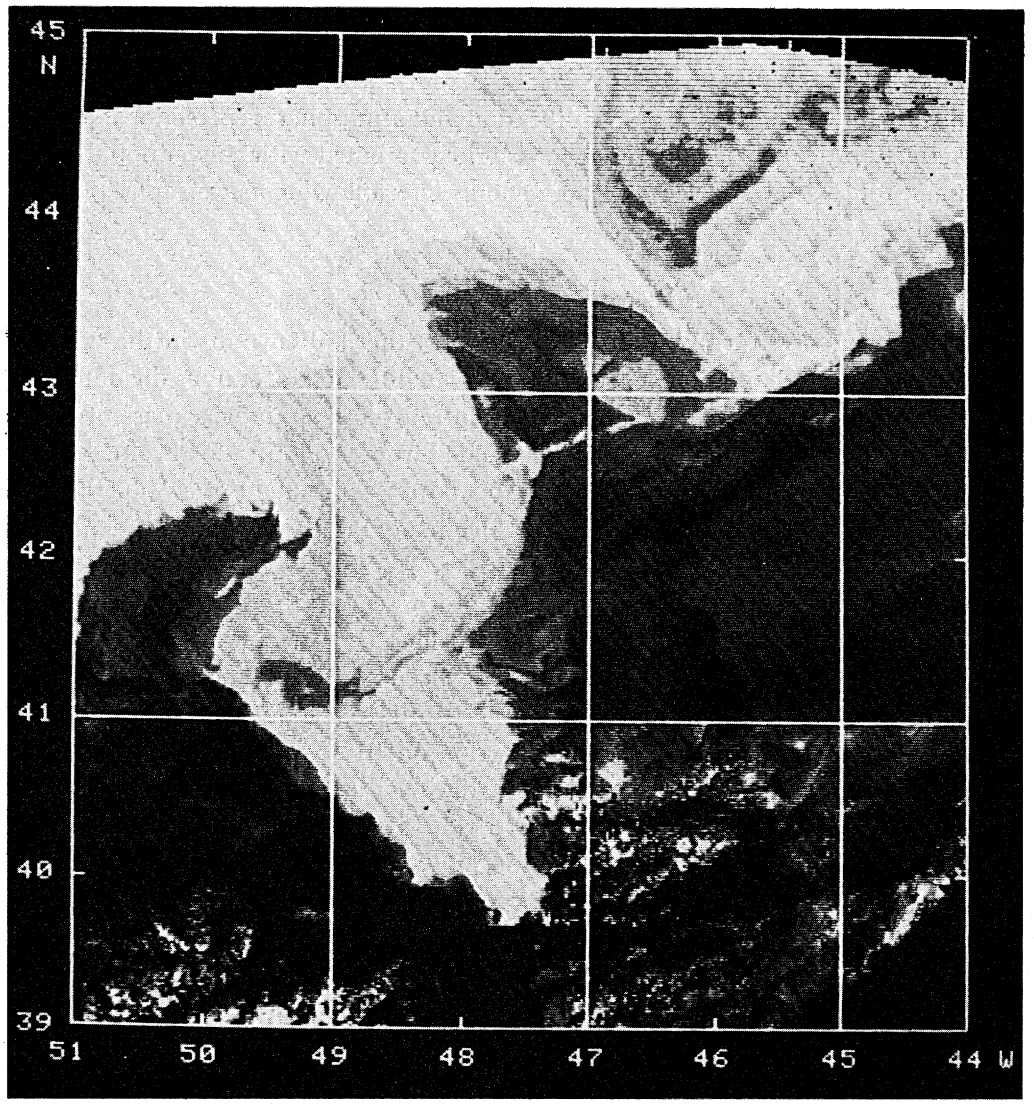

FIGURE 9. The four *TIROS-N* images in figure 6 merged into a composite designed to minimize the effect of clouds. The composite was formed by comparing the temperatures for four days at each pixel location and retaining the warmest temperature at each address for those four days (Holyer *et al.* 1980).

in the polar regions are fast moving, the chances are increased of a satellite passing over a cloud-free period during a given day. Compositing the several passes that occur in 1 or 2 days can minimize the amount of ocean change that may have taken place.

An expansion of the compositing method developed by La Violette & Chabot (1969) uses a sliding composite technique (Holyer *et al.* 1980). In this method, a selected number of days are composited to form the first of a series of images. The next composite image uses the same number of days, but drops the first day and adds the next chronological day to the series. The resulting composite image is, thus, one day removed from the first composite image. The method is continued until a satisfactory series that can be made into a loop cine is made. One potential application of this technique is to make loop movies of satellite imagery to compare with cine loops derived from numerical models.

PHILOSOPHICAL TRANSACTIONS OF THE ROYAL SOCIETY A MATHEMATICAL, PHYSICAL & ENGINEERING SCIENCES

Examples of oceanographic analysis using processed satellite image and conventional data

If the basic functions (i.e. registration, calibration and atmospheric corrections) are properly done, interactively processed satellite imagery can be combined with conventional ocean data in the oceanographic analysis of an ocean region. The following paragraphs present some typical examples.

The Grand Banks experiment

This experiment involved a two-year ocean study of thermal currents in the waters of the Grand Banks of Newfoundland. The field work used satellites and aircraft as the data collection platforms. The May 1979 portion of the study centred on examining a mass of cold water 350 km long and 100 km wide that had been extruded from the Labrador Front. Much of the following was taken from the results of the Grand Banks experiment (La Violette 1981; La Violette 1983). The satellite used was *TIROS-N*, the first of the NOAA satellites equipped with AVHRR.

On 16 May, a frontal survey, which consisted of a research aircraft flying sorties along a right-angle cut across the cold feature, was made. The aircraft operation flight lines were determined by 15 May *TIROS-N* imagery that had been registered and enhanced before the flight. Analysis of the aircraft data produced a vertical cross section of the atmospheric and oceanic conditions in one portion of the study region on 16 May.

To relate this comparatively narrow view to the overall regional conditions, *TIROS-N* infrared data were registered and enhanced, and a plot of the aircraft survey track was overlaid on the image shown in figure 10*a*. The figure also shows an ocean cross section produced from aircraft expendable bathythermographs (AXBTS). The cross section indicates that the cold water in the satellite image is not the surface spreading of windblown, low-density water, but is a large major extrusion that extends into the water column deeper than 350 m. Surface currents were plotted by using the rate and direction of drifting sonobuoys dropped from the aircraft (figure 10*b*).

The regional circulation over a period of four days (including the 16 May aircraft survey) was also studied using *TIROS-N* imagery (figure 6). Because of the registration precision, day-to-day movements along the front could be studied and accurately measured. Within the cold water to the north, filaments of cold water are shown to be rapidly moving about the feature. Although the day-to-day shape of the filaments became distorted, they showed a surprising ability to retain their identity.

The Donde Va? experiment

The purpose of Donde Va? was to define the variability and the causes of the surface circulation in the Alboran Sea (La Violette *et al.* 1982; Kinder 1983; The Donde Va? Group 1984). In addition to the satellite data, the experiment involved aircraft, ships and moored buoy data.

The twice-daily passes of the *NOAA-7* over the study area permitted almost continuous monitoring of the surface thermal changes that occurred in the Alboran Sea during the period when intensive air and sea measurements were being conducted (October 1982). The satellite infrared imagery showed that a number of submesoscale cold-water features were being

PHILOSOPHICAL TRANSACTIONS OF THE ROYAL SOCIETY A MATHEMATICAL, PHYSICAL & ENGINEERING SCIENCES

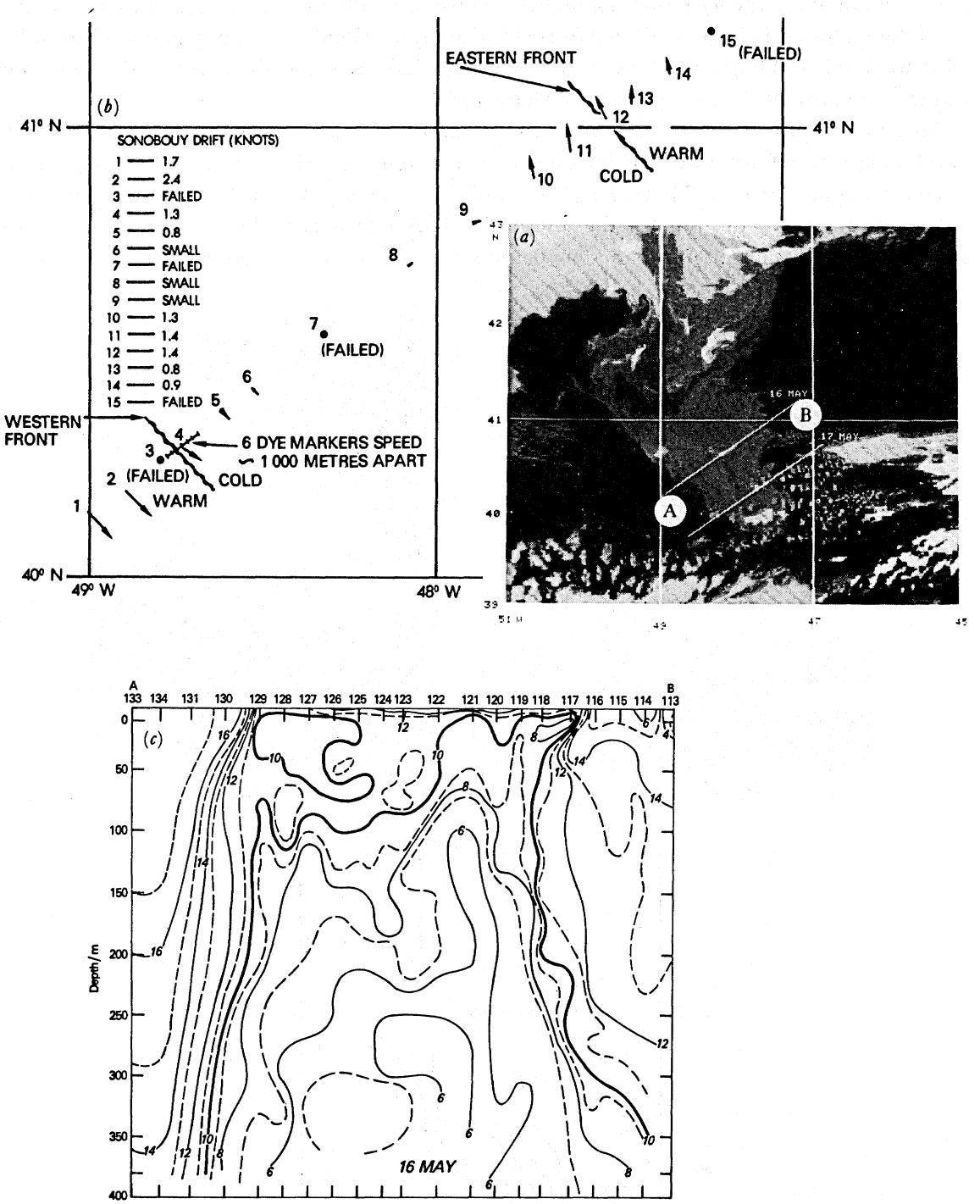

FIGURE 10. (*a*) *TIROS-N* image for 16 May 1979. Line for 16 May refers to location of sonobuoy and XBT front survey. (Lower line refers to a second airborne survey that is not shown here.) (*b*) Drift vectors based on sonobuoy data. (*c*) Temperature vertical cross section based on airborne XBT data. Numbers between A and B refer to station numbers and positions of airborne XBTs (La Violette 1983).

PHILOSOPHICAL TRANSACTIONS OF THE ROYAL SOCIETY A MATHEMATICAL, PHYSICAL & ENGINEERING SCIENCES

advected about a large gyre that dominated the western Alboran (figure 7). The examination of satellite infrared imagery collected during the one-year Donde Va? study period (November 1981 to October 1982), as well as from other years, indicates that these mesoscale cold-water features are normal for the gyre (La Violette 1984).

An enlargement of the IR image for 15h01 on 12 October showed a cold-water feature developing east of Gibraltar. The image is shown in figure 11 with a CZCS visible image of the same area approximately 3 h earlier (11h55) of the same day. From the time of the morning NOAA IR image to the time of the afternoon NOAA IR image (11 h), the feature moved 16.7 km at an average of approximately 0.4 m s^{-1}. The CZCS image, however, indicated that a

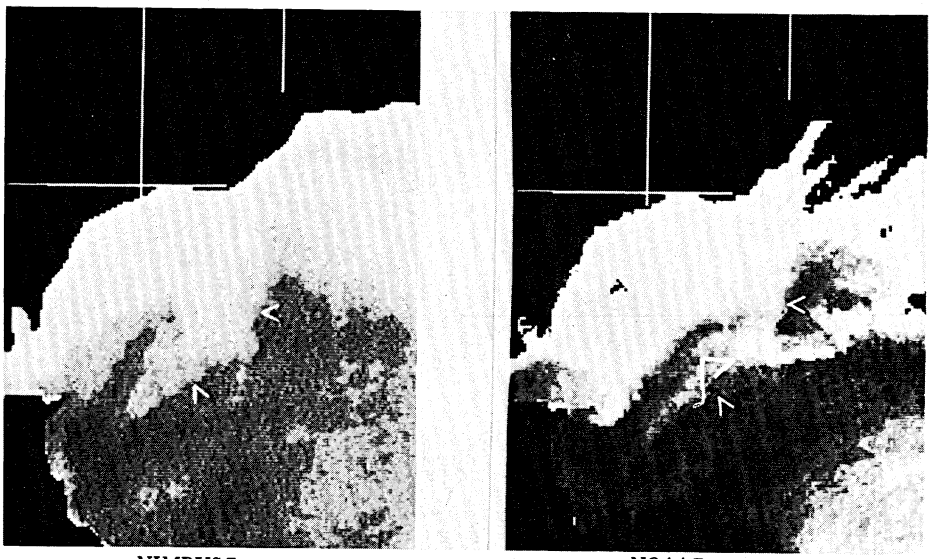

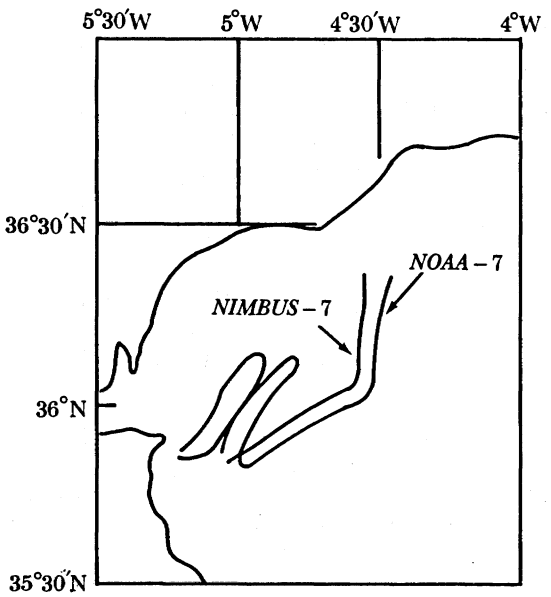

FIGURE 11. The detection of tide-current-related, short-term movement of a cold-water feature in the Alboran Sea by using Mercator-registered *Nimbus* CZCS and *NOAA*-7 AVHRR-IR imagery. The movement of approximately 9 km took place between 11h55 (*Nimbus* image) and 15h01 (NOAA image) on 12 October 1982 (La Violette 1984).

movement of approximately 9 km occurred in the time between the *Nimbus* noon pass and NOAA afternoon pass. This equates to a movement of 0.8 m s^{-1}, or twice the rate of movement for the period of 11 h between the two NOAA images.

When the data were compared with the tide tables of the region, the time of the spurt in speed of the feature was found to correspond to the time of the maximum eastward component of the tidal current. This and other satellite and conventional data indicated a strong influence of the tidal currents in the circulation of the upper 200 m of water in the western Alboran Sea (La Violette & Lacombe 1987).

In a study of the drift rate of sonobuoys dropped from a research aircraft during 9 through

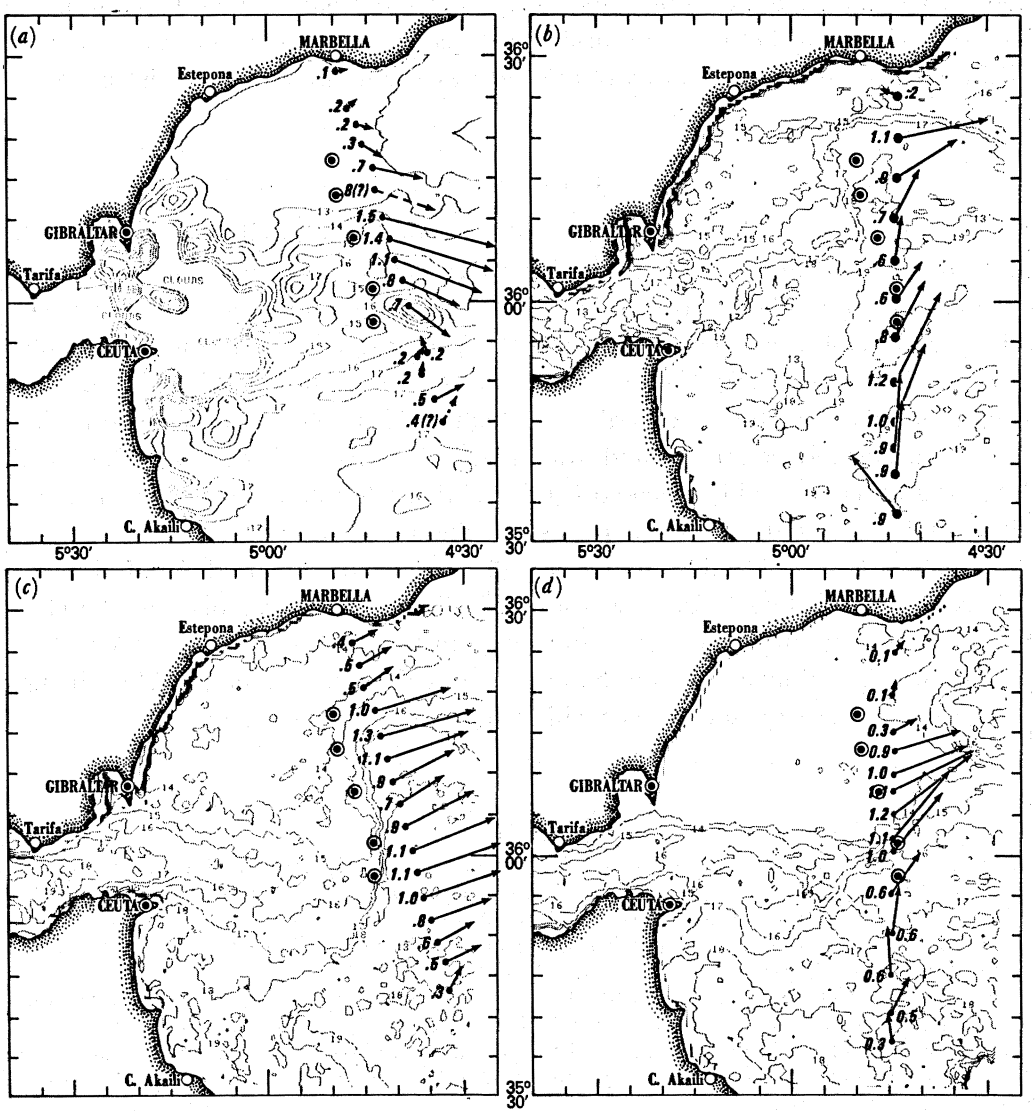

FIGURE 12. The positions of short-term sonobuoy drift movements (in metres per second) in relation to the sea-surface temperature field devised from *NOAA*-7 AVHRR IR data during the Donde Va? experiment. The circled dots refer to a line of current meter moorings also in position at that time. This is an example of how field-collected data can be integrated with accurately Mercator-registered and atmospherically corrected satellite imagery (after La Violette 1986). (*a*) Start 10h25, finish 15h15, average time 04h30 min; (*b*) start 09h17, finish 13h21, average time 03h48 min; (*c*) start 09h58, finish 15h58, average time 5h38 min; (*d*) start 09h30, finish 13h46, average time 3h45 min.

18 October, La Violette (1986) showed that surface currents associated with the incoming Atlantic water flowed at speeds equal to or greater than 1.0 m s^{-1} and that, on the average, the greatest speeds (i.e. speeds of 1.2 m s^{-1}) were limited to a band less than 16 km wide centred approximately between the 17 and 18 °C surface isotherm. Of interest is the fact that the band of fast-moving surface water flowed just inside the periphery of the advected cold-water features shown in the satellite imagery (figure 12).

Comparing the average drift speed of the sonobuoys (*ca.* 1.2 m s^{-1}) at the periphery with the average advection speed of the cold-water feature (0.4 m s^{-1}) gave an indication of the differences between the surface currents and the translation speed of the feature around the gyre. Comparison of current speeds derived from sonobuoys dropped in the southeastern part of the gyre on 18 October and the translation speeds derived from 18 and 19 October imagery revealed that although the sonobuoy drift speed decreased sharply from the velocities found near Gibraltar, the translation speed of the features essentially remained the same.

Conclusions

Certain basic image analysis techniques must be applied to satellite data so that this form of data will be a reliable and quantitative source of oceanographic information. Proper registration and atmospheric correction are the most important of these basic techniques (especially with visible range data where up to 90 % of the signal may be due to the intervention of the atmosphere). Also, registration to a set graphic projection can be extremely useful in allowing several days of data to be studied as a temporal, as well as a spatial, continuity. When the data are accurately calibrated and atmospherically corrected, however, the usefulness of the data expands considerably when coregistered with other data sets and used as part of an overall analysis of the data available for a study region.

The specific concepts of understanding a study region's oceanography and of knowing the limitations of satellite data cannot be overemphasized. These concepts must be clear to an investigator before computer-processed imagery can be properly exploited. With this knowledge and with the utilization of the basic image analysis techniques, satellite imagery can provide an imaginative oceanographer with a powerful analytical tool.

References

Arnone, R. A. 1983*a* Evaluation of czcs and *LANDSAT* for coastal optical and water properties. In *17th International Symposium on Remote Sensing of the Environment, San Jose, Costa Rica, April 23–30 1980*. Ann Arbor, Michigan: Environmental Research Institute of Michigan.

Arnone, R. A. 1983*b* Water optics of the Mississippi sound. Naval Ocean Research and Development Activity, NSTL, Mississippi, report 63.

Arnone, R. A. & La Violette, P. E. 1984 A method of selecting optimal Ångstrom coefficients to obtain quantitative ocean color data from Nimbus 7 CZCS. *SPIE*, vol. 489 (Ocean Optics VII), pp. 187–194.

Arnone, R. A. & La Violette, P. E. 1986 Bio- and chem-optical variability of the shear eddies associated with the African Current off Algeria as assessed by the *Nimbus*-7 coastal zone color scanner. *J. geophys. Res.* **91**, 2351–2364.

Austin, R. W. & Petzold, T. J. 1980 The determination of the diffuse attenuation coefficient of sea water using the coastal zone colour scanner. In *Oceanography from space* (ed. J. F. R. Gower), p. 239. New York: Plenum Press.

Clark, R. & La Violette, P. E. 1981 Detecting the movement of oceanic fronts using registered TIROS-N imagery. *Geophys. Res. Lett.* **8**, 229–232.

Donde Va? Group 1984 Donde Va? An oceanographic experiment in the Alboran Sea. *Eos, Wash.* **65** (36), 682–683.

PHILOSOPHICAL TRANSACTIONS OF THE ROYAL SOCIETY A MATHEMATICAL, PHYSICAL & ENGINEERING SCIENCES

Gordon, H. R. 1978 Removal of atmospheric effects from satellite imagery of the oceans. *Appl. Opt.* **17**, 1631–1636.
Gordon, H. R. & Clark, D. K. 1980*a* Atmospheric effects in remote sensing of phytoplankton pigments. *Bound.-Layer Met.* **18**, 299–313.
Gordon, H. R. & Clark, D. K. 1980*b* Remote sensing optical properties of a stratified ocean: an improved interpretation. *Appl. Opt.* **19**, 3428.
Gordon, H. R. & Clark, D. K. 1981 Clear water radiances for atmospheric correction of coastal zone color scanner imagery. *Appl. Opt.* **20**, 4175–4180.
Gordon, H. R. & McCluny, W. R. 1975 Estimation of the depth of sunlight penetration in the sea in remote sensing. *Appl. Opt.* **14**, 413–446.
Gordon, H. R., Brown, V. W., Brown, O. B., Evans, R. H. & Clark, D. K. 1983 *Nimbus*-7 czcs: reduction of its radiometric sensibility with time. *Appl. Opt.* **22**, 3929.
Holter, M. 1970 Imaging with nonphotographic sensors. In *Remote sensing with special reference to agriculture and forestry*, ch. 3. Washington, D.C.: National Academy of Sciences.
Holyer, R. J., La Violette, P. E. & Clark, J. R. 1980 Satellite oceanography research, development, and technology transfer. In *Proc. 14th Int. Symposium on Remote Sensing of the Environment, San Jose, Costa Rica, April 23–30 1980*. Ann Arbor, Michigan: Environmental Research Institute of Michigan.
Hovis, W. A., Clark, D. K., Anderson, F., Austin, R. W., Wilson, W. A., Butler, E. I., Ball, D., Gordon, H. R., Mueller, J. L., El-Sayed, S. F., Sturm, B., Wrigley, R. C. & Yentsch, C. 1980 *Nimbus*-7 Coastal Zone Color Scanner: system description and initial imagery. *Science, Wash.* **210**, 60–63.
Hussey, W. J. 1979 The *TIROS-N/NOAA* operational satellite system. National Environmental Satellite Service/*NOAA*, Washington, D.C., *NOAA NESS* tech. memo 95, 35 pp.
Kinder, T. H. 1983 Donde Va? An oceanographic experiment near the Strait of Gibraltar. In *Proceedings of IAPSO/ONR/NEFKD Workshop on Straits*. Copenhagen: Inst. Phys. Ocean.
La Violette, P. E. 1981 Variations in the frontal structure of the southeastern grand banks. Naval Ocean Research and Development Activity, NSTL-Bay St. Louis, Mississippi, report 87, 48 pp.
La Violette, P. E. 1983 The Grand Banks experiment: a satellite/aircraft/ship experiment to explore the ability of specialized radars to define ocean fronts. Naval Ocean Research and Development Activity, NSTL-Bay St Louis, Mississippi, report 49, 126 pp.
La Violette, P. E. 1984 The advection of the submesoscale thermal features in the Alboran Sea gyre. *J. phys. Oceanogr.* **14**, 550–565.
La Violette, P. E. 1986 Short-term measurements of the velocity of currents associated with the Alboran Sea Gyre during Donde Va?. *J. phys. Oceanogr.* **16**, 262–279.
La Violette, P. E. & Chabot, P. L. 1969 A method of eliminating cloud interference in satellite studies of sea surface temperature. *Deep Sea Res.* **16**, 534–547.
La Violette, P. E., Kinder, T. H., Preller, R. & Hurlburt, H. E. 1982 Donde Va?: a mesoscale flow dynamics experiment in the Strait of Gibraltar and Alboran Sea. In *Proc. 28th Congress and Plenary Assembly of CEISM, Cannes,* 2–11 December.
La Violette, P. E. & Lacombe, H. 1988 Tidal-induced pulses in the flow through the Strait of Gibraltar. *Oceanol. Acta.* (In the press.)
McClain, E. P., Pichel, W. G., Walton, C. C., Ahmad, Z. & Sutton, J. 1977 Multichannel improvements to satellite-derived global sea surface temperatures. *Adv. Space Res.* **2**, 43–47.
Schwalb, A. 1978 Modified revisions of the improved TIROS Operations (ITOS D-G). National Environmental Satellite Service/*NOAA*, Washington, D.C., *NOAA NESS* tech. memo *NESS* 35, 48 pp.
Smith, R. C. & Wilson, W. H. 1981 Ship and satellite bio-optical research in the California bight. In *Oceanography from space* (ed. J. F. R. Gower), p. 281. New York: Plenum Press.

Discussion

J.-P. A. L. Muller (*Department of Photogrammetry and Surveying, University College London, U.K.*). How far has the understanding of satellite oceanographic images advanced the knowledge of what the flows seen in satellite image sequences actually represent in terms of surface currents and circulation? In particular, are there any quantitative models which reproduce the satellite flow fields observed?

P. E. La Violette. As I have tried to emphasize, the features seen in the imagery are tracers of the circulation and are not direct measurements *per se*. If used judiciously in this regard, then the direction of currents (but not their speed) and the displacement (including rate of

PHILOSOPHICAL TRANSACTIONS OF THE ROYAL SOCIETY A MATHEMATICAL, PHYSICAL & ENGINEERING SCIENCES

displacement) and variation of circulation features can be accurately inferred. For example, the monitoring of satellite-derived turbulent jets and eddies associated with the California current system have identified these features as crucial to the cross-shore transport. Their variance seasonally has been shown to be a direct result of seasonal changes in the velocity structure of the California current (see, for example, Kosro & Huyer 1986). Similar work with satellite imagery has been done to derive the circulation structure of multiple dipole eddies in the Alaska coastal current (Ahlnas *et al.* 1987). The ability of the movement of circulation features in successive imagery to act as lagrangian drifters is a more direct application of these imagery studies (Kelly 1983, 1985). There are problems with this in that the events are moving vertically as well as horizontally and that translation speeds of the features can be confused with current speed. Much of the early work by this method (see, for example, La Violette 1984; Vastano & Borders 1984; Vastano & Reid 1985) was done manually and is operator subjective. Objective computer techniques that use sea surface velocities are just now starting to be developed (see, for example, Emery *et al.* 1986). This developing methodology, used with constraints such as I have tried to emphasize in my paper (this symposium) promises to become an extremely powerful tool in satellite ocean research.

References

Ahlnas, K., Royer, T. H. & George, T. H. 1987 *J. geophys. Res.* **92** (C12), 13041–13047.

Emery, W. J., Thomas, A. C., Collins, M. J., Crawford, W. R. & Mackas, D. L. 1986 *J. geophys. Res.* **91**, 12865–12879.

Kosro, P. J. & Huyer, A. 1986 In *CTD and velocity surveys of seaward jets of northern California, July 1981 and 1982* (*J. geophys. Res.* **91**), pp. 7680–7690.

La Violette, P. E. 1984 *J. phys. Oceanogr.* **14**, 450–505.

Vastano, A. C. & Borders, S. E. 1984 *Remote Sens. Environ.* **16**, 87–90.

Vastano, A. C. & Reid, R. O. 1985 *J. atmos. Technol.* **2**, 393–400.

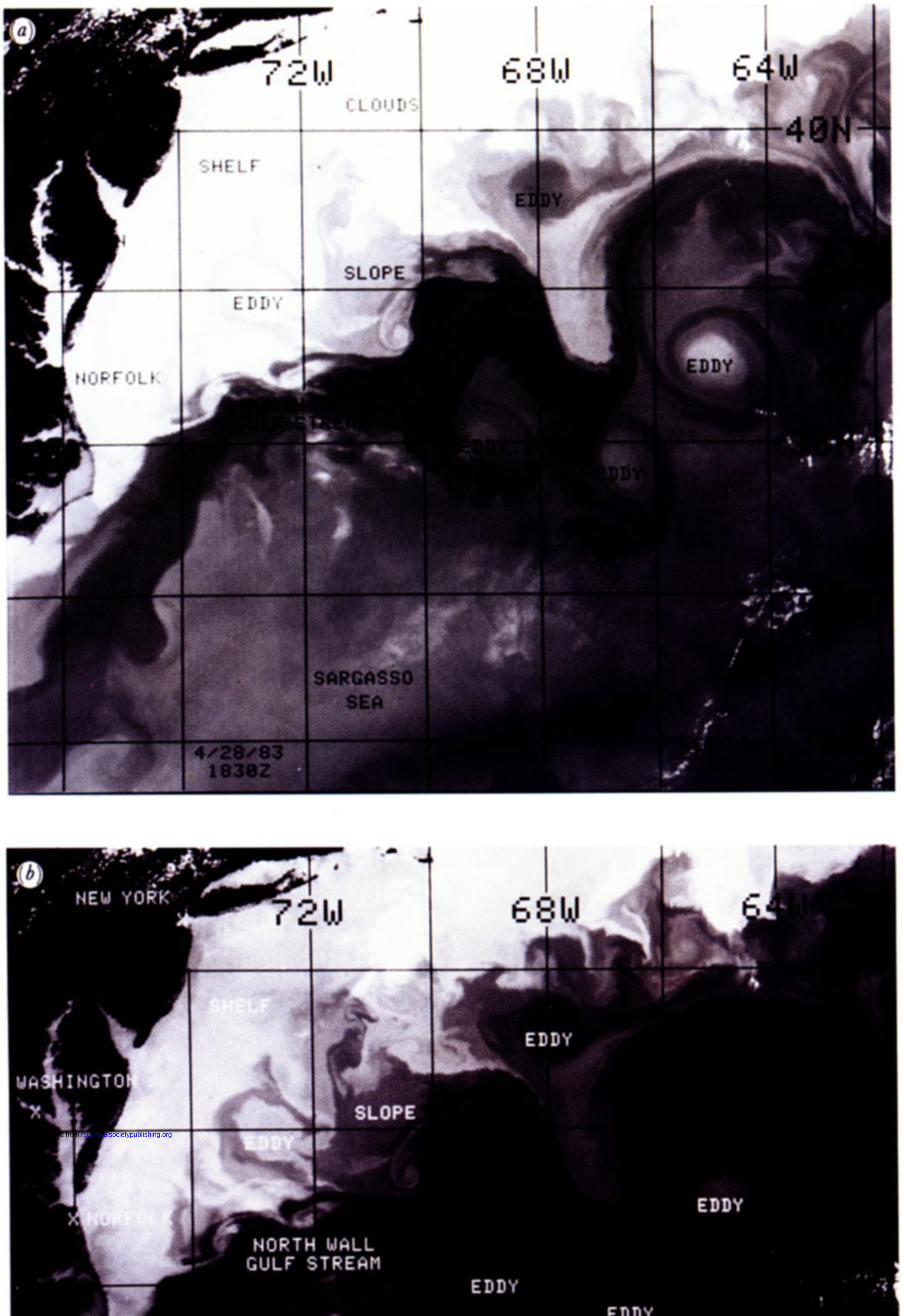

FIGURE 1. (*a*) This cloud-free *NOAA*-7 AVHRR IR (channel 4, i.e. 10.3–11.3 μm) image of the eastern seaboard of the United States was taken on 28 April 1983. The registered, calibrated image shows the thermal convolutions of the Gulf Stream as it forms a border between the warmer waters of the Sargasso Sea and the coastal cold slope waters off the continental shelf (the darker portions of the picture are the warmer radiated temperatures of the scene).

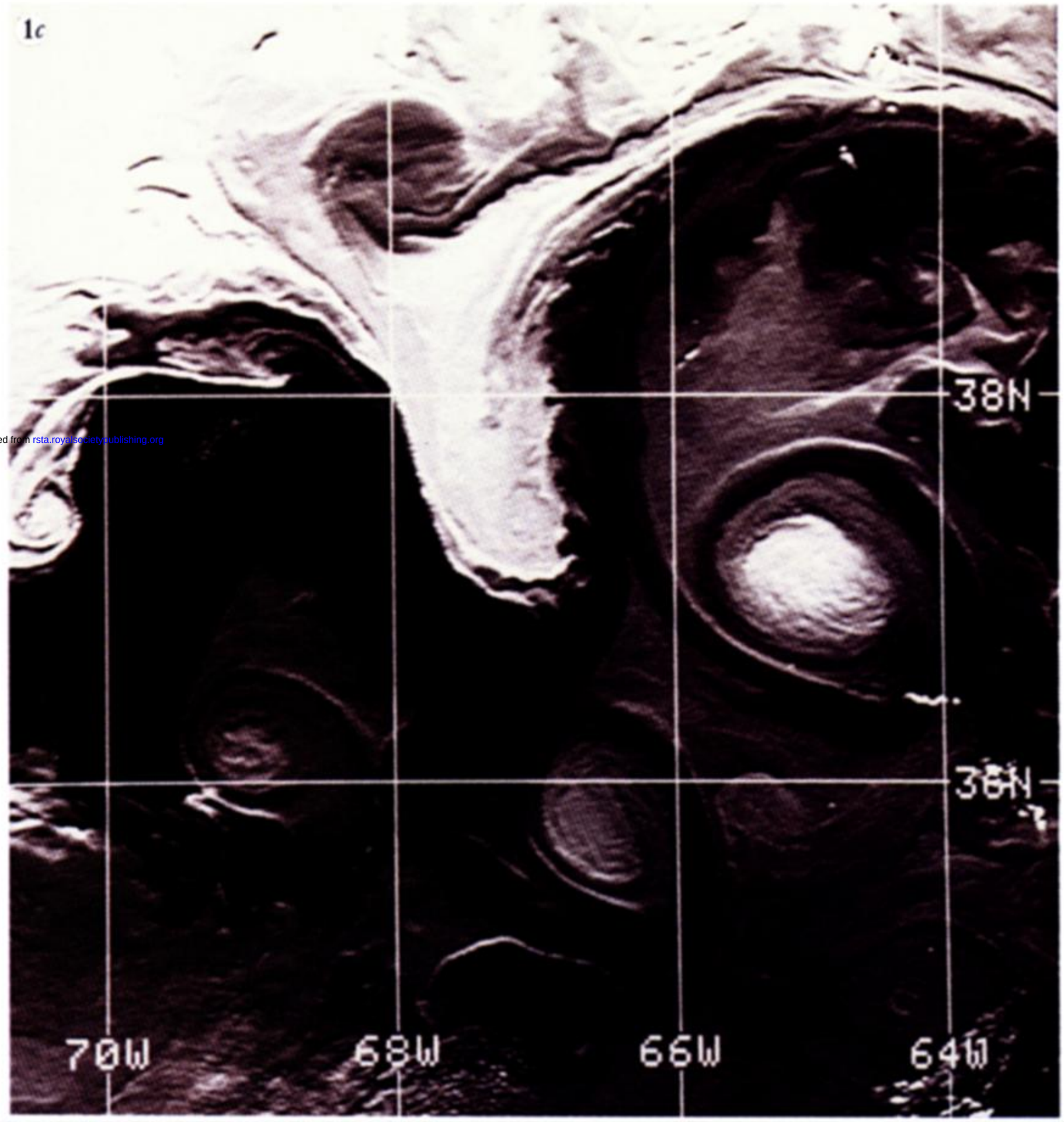

FIGURE 1. (*c*) This higher resolution (1 km) subsection of figure 1*a* was processed with a modified Frei-Chen edge enhancement filter. Filter weights were chosen so that the intensity at each point was replaced by a 3×3 finite difference approximation to the original image. Linear contrast enhancement was applied to the image before the filtering. The results show the impression of relief based on the sea surface temperatures. The relief is the opposite of reality in that the white (cold-core) rings should represent a depression in the ocean surface and not a rise. (Photograph courtesy of Matthew Lybanon, NORDA.)

PHILOSOPHICAL TRANSACTIONS OF THE ROYAL SOCIETY A MATHEMATICAL, PHYSICAL & ENGINEERING SCIENCES

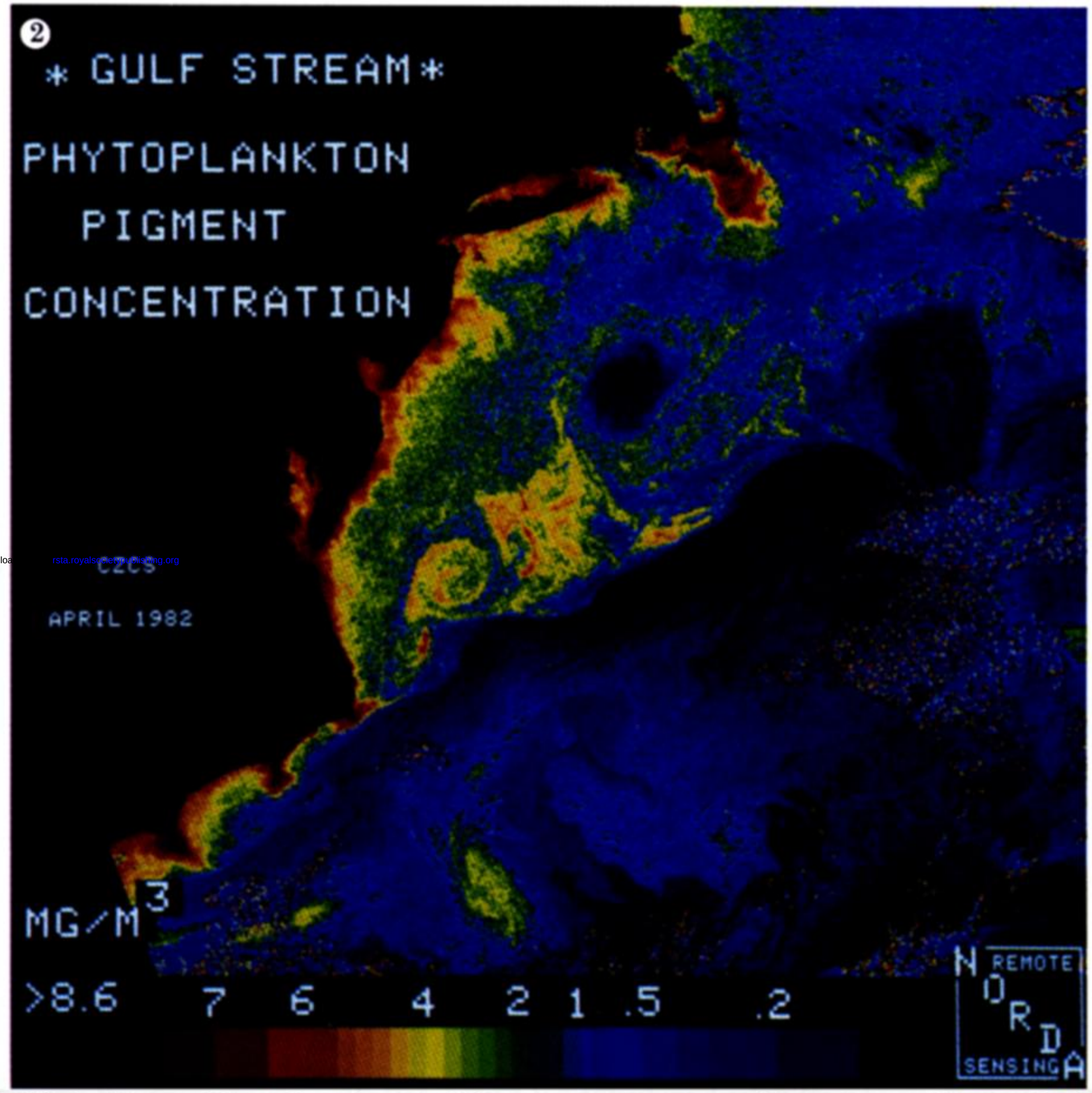

FIGURE 2. This *Nimbus* 7 CZCS false-colour image of the same ocean area as figure 1 was taken on 24 April 1982. In this instance, the registered, calibrated image has been atmospherically corrected and presents colour variations representing values that result from ratioing the CZCS 450 and 550 spectral channels. Although the values derived from this ratio are normally used to show the chlorophyll distribution in the ocean, here they are equally instructive in showing the region's current and frontal distribution. Note that the temperature values presented as grey tones in figures 1*a*, *b* could also have been displayed in colour in the way shown here. The advantage of colour goes beyond aesthetics in that the colour scale can show a greater range than the black and white scale. A case in point is that the details of the ocean features northwest of the Gulf Stream are clearly shown in this figure, whereas they had to be added as a subimage in figure 1. (Photograph courtesy of Robert A. Arnone, NORDA.)

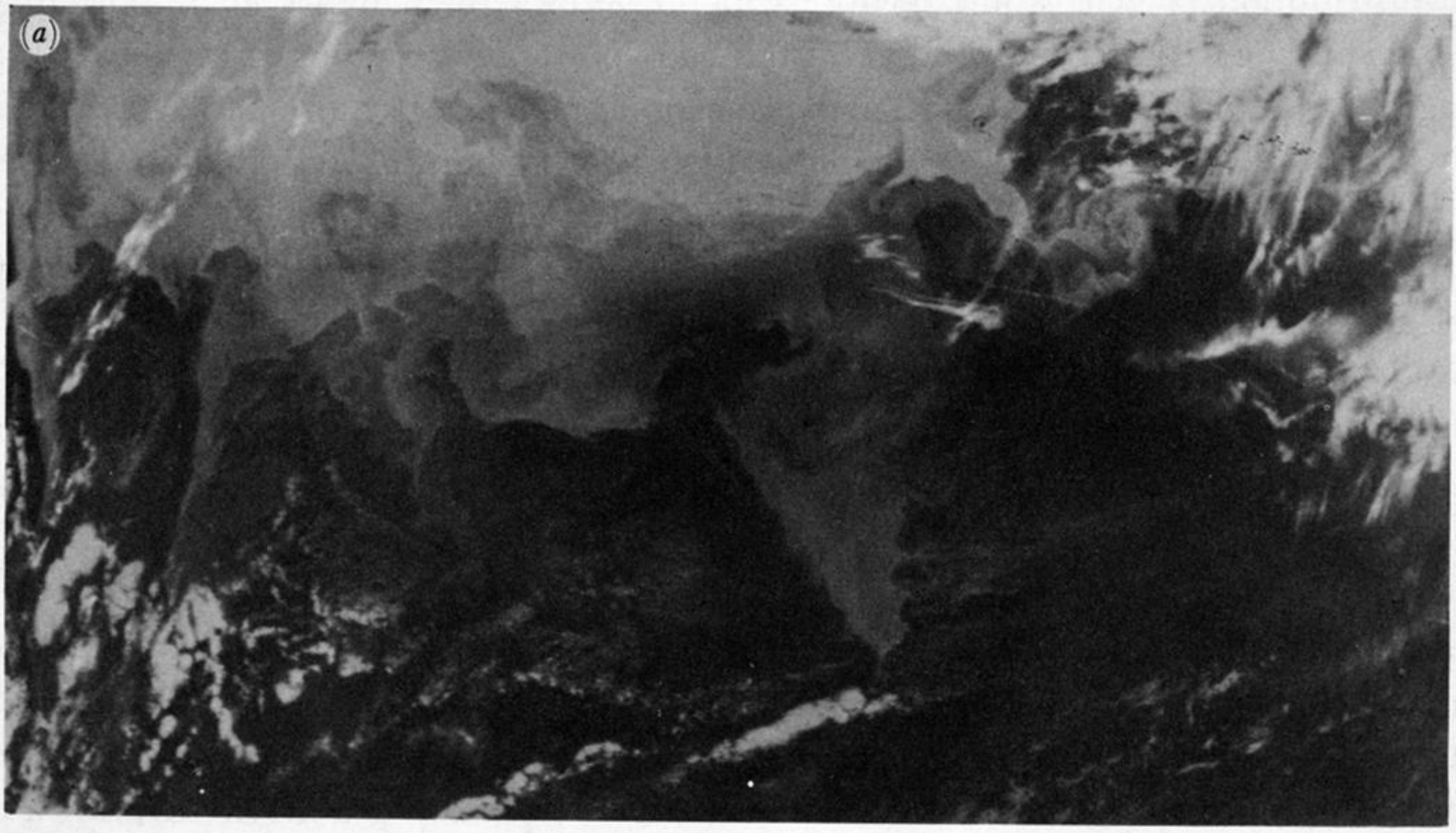

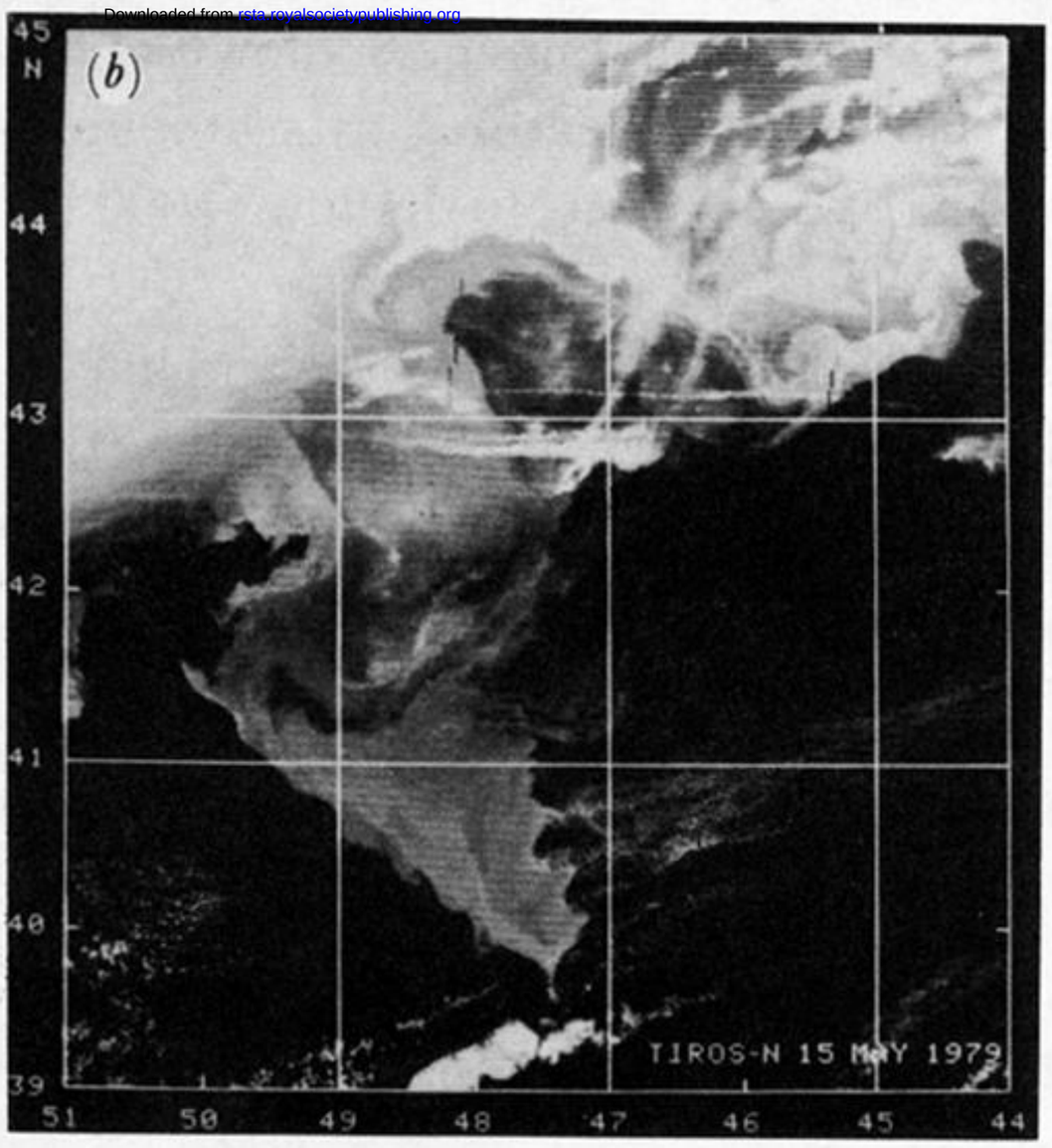

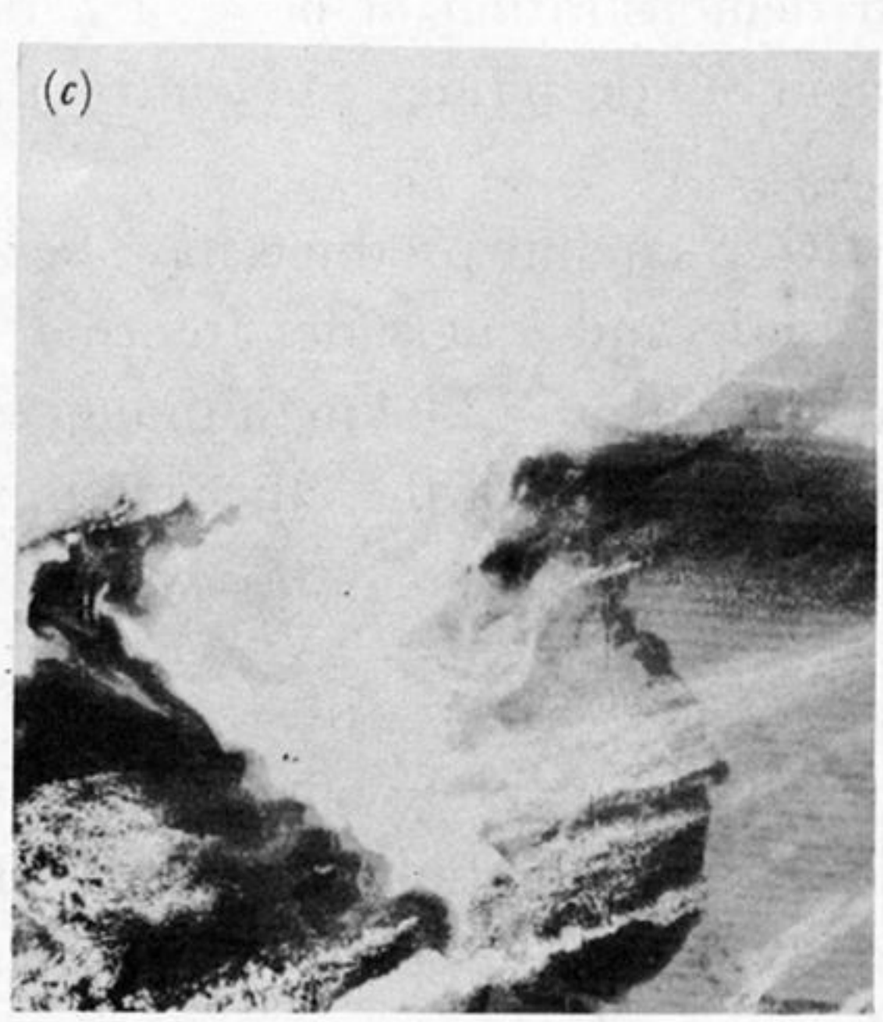

FIGURE 5. (*a*) Standard *TIROS-N* infrared (10.5–11.5 μm) image product from NOAA/NESDIS for 15 May 1979 showing the meandering pattern of the Gulf Stream southeast of Newfoundland, Canada. (*b*), (*c*) Two enhancements of Mercator-registered imagery of the 15 May 1979 *TIROS-N* infrared image shown in (*a*) to show various aspects of a cohesive mass of cold water that extruded into the eastward path of the Gulf Stream. Details of the cold-water extrusion are shown in (*b*), and details of the northward movement of warm water (Gulf Stream) into the eastern section of the area are shown in (*c*) (Holyer *et al.* 1980).

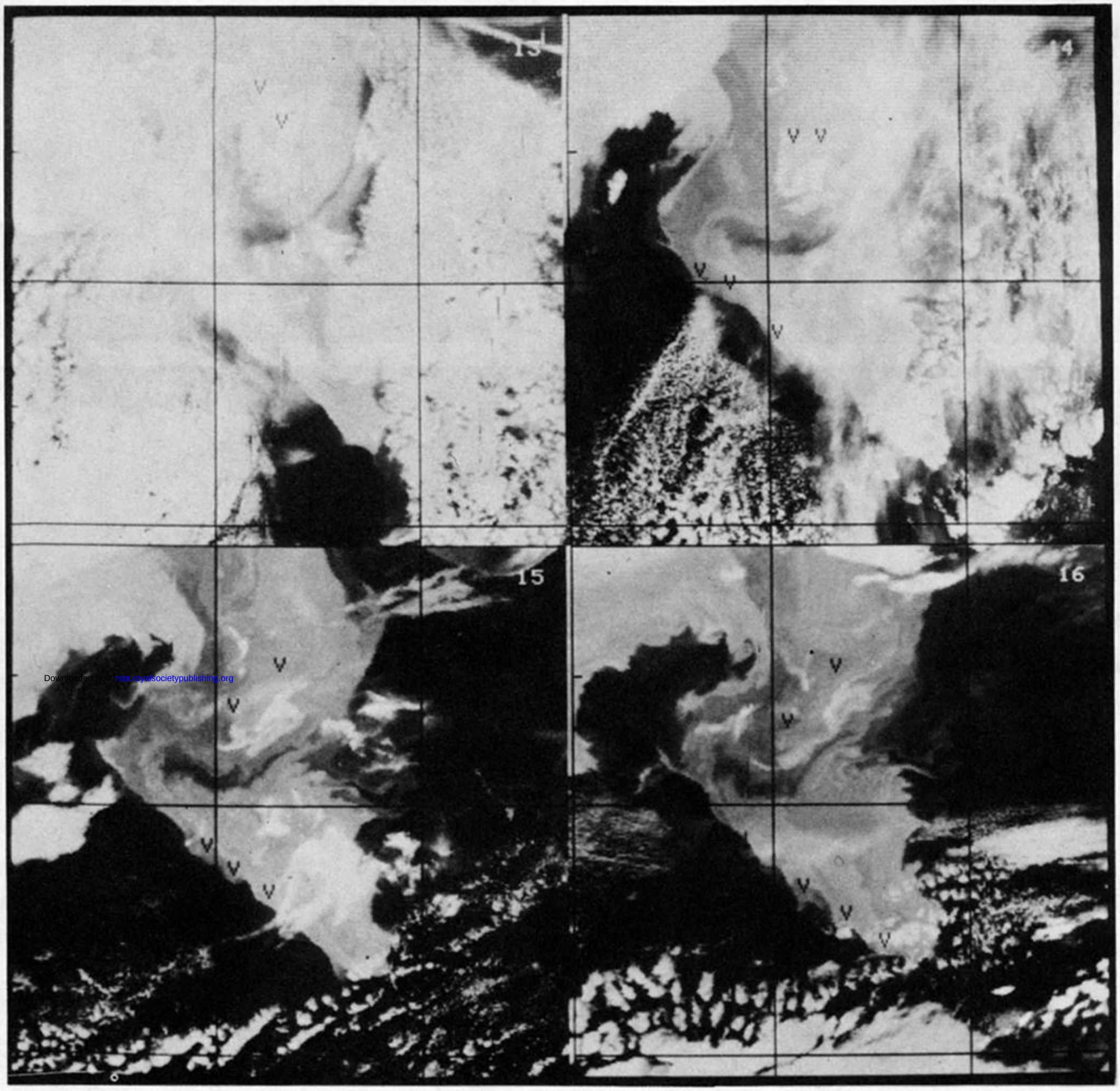

FIGURE 6. Mercator-registered *TIROS-N* infrared (10.5–11.5 μm) imagery of the waters of the Grand Banks southeast of Newfoundland, Canada, for four successive days in May 1979 (the series includes the image in figure 5). The imagery shows the movement of frontal shear waves moving along the boundaries of a cohesive mass of cold water that had been extruded into the eastward path of the Gulf Stream. The shear waves were active on both the western and eastern fronts of the cold-water mass and moved at phase speeds of approximately 70 cm s^{-1}, a period of approximately 0.83 days and a wavelength of 50 km. Movement during a period of 12 hours is marked by arrows. A comparison of these derived phase speeds with *in situ* measured current speeds shows the waves were moving at nearly the same speed as the cold-water currents. The imagery shows that rapid movement within the ridge feature was also measurable. Tracking the displacement of several cold filaments within the cold water over several days shows they averaged 70 cm s^{-1}. These displacements are similar to velocities measured by satellite drifter buoys tracked during the same period. The imagery has not been atmospherically corrected (La Violette 1983).

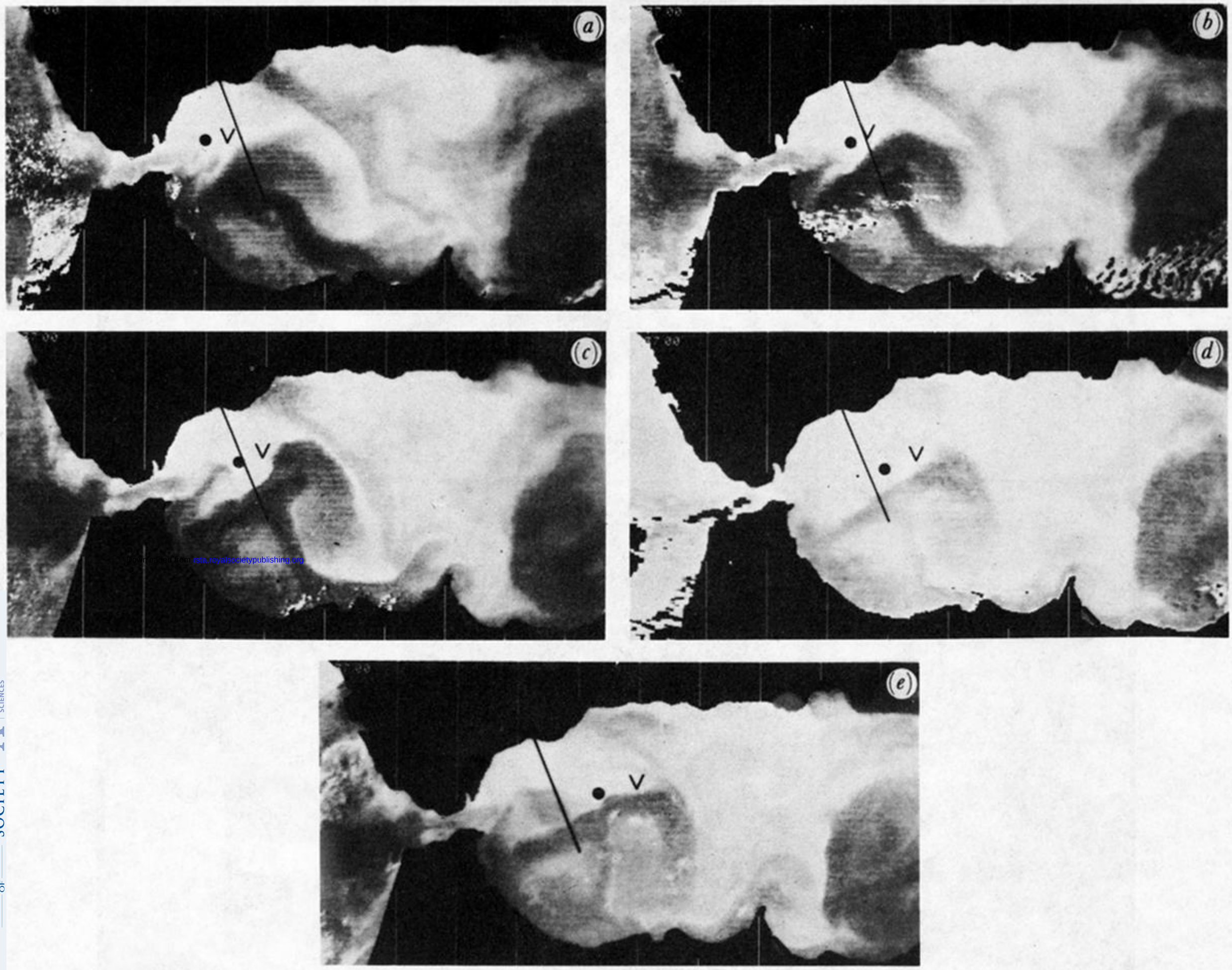

FIGURE 7. *NOAA*-7 AVHRR-IR imagery of the Alboran Sea collected as part of the Donde Va? experiment during October 1982. The dot and the 'V' in the images show the advection of two submesoscale cold features about the permanent gyre located in the Alboran Sea. The black line represents a line of current meter moorings positioned during the Donde Va? experiment. A close examination of the imagery shows that other unmarked features were also being advected and that their generation was probably tide related. Continuous monitoring of these cold-water features was possible because of the twice-daily (about every 12 h) spacing of the *NOAA*-7 overpasses. After registration to a Mercator projection (accuracy ± 1 km) and an atmospheric correction to arrive at absolute temperatures, analysis of the displacement of the cold features in successive images shows their apparent origin east of Gibraltar, their average speeds of 40 cm s^{-1} around the gyre, and their apparent entrailment into the incoming Atlantic water east of Gibraltar (La Violette 1984). (*a*) 14h32 GMT 6 October; (*b*) 02h56 GMT 7 October; (*c*) 14h22 GMT 7 October; (*d*) 02h44 GMT 8 October; (*e*) 14h08 GMT 8 October.

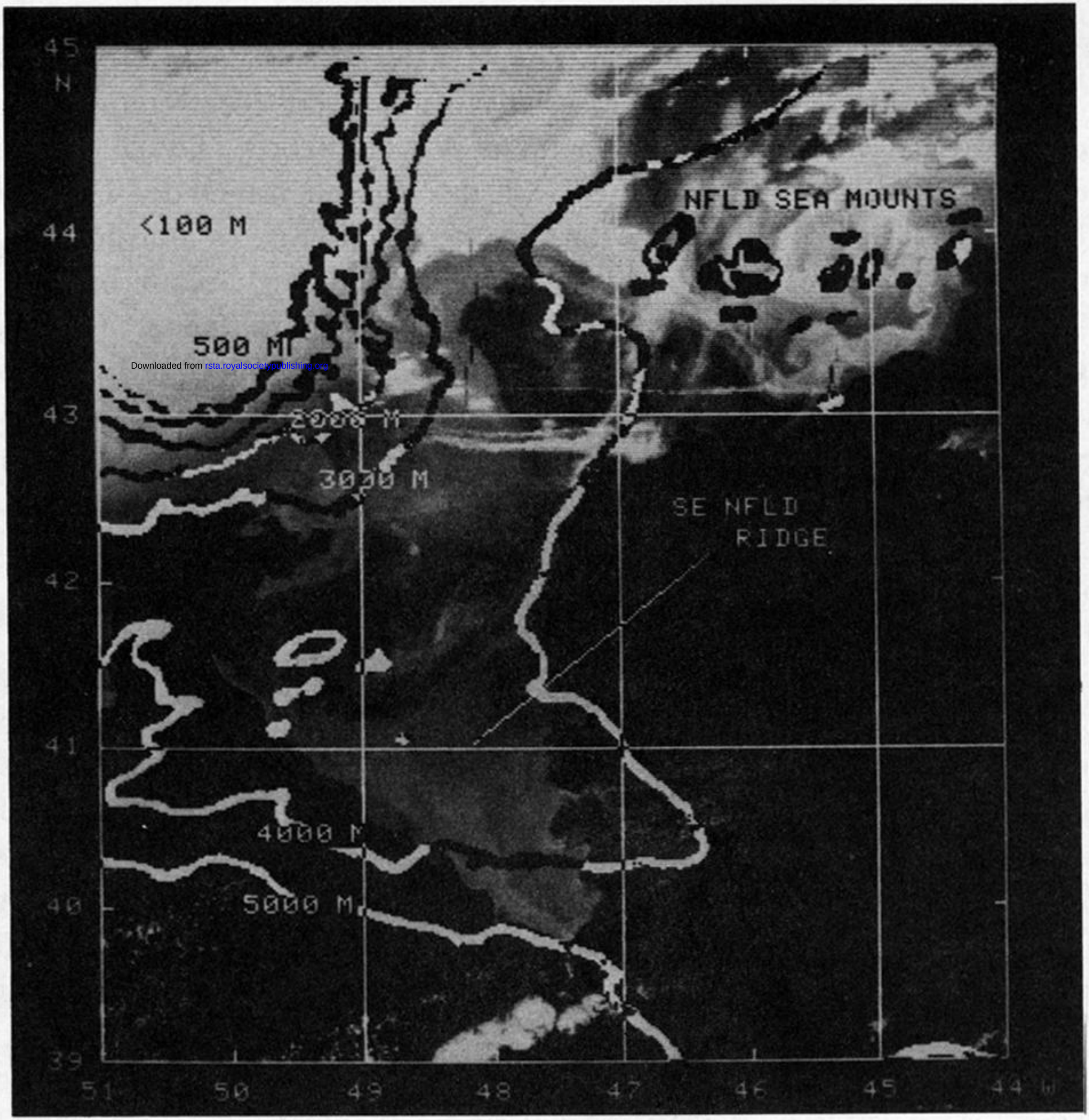

FIGURE 8. *TIROS-N* image for 15 May 1979 overlain with the 500, 1000, 2000, 3000, 4000, and 5000 m isobaths (Holyer *et al.* 1980).

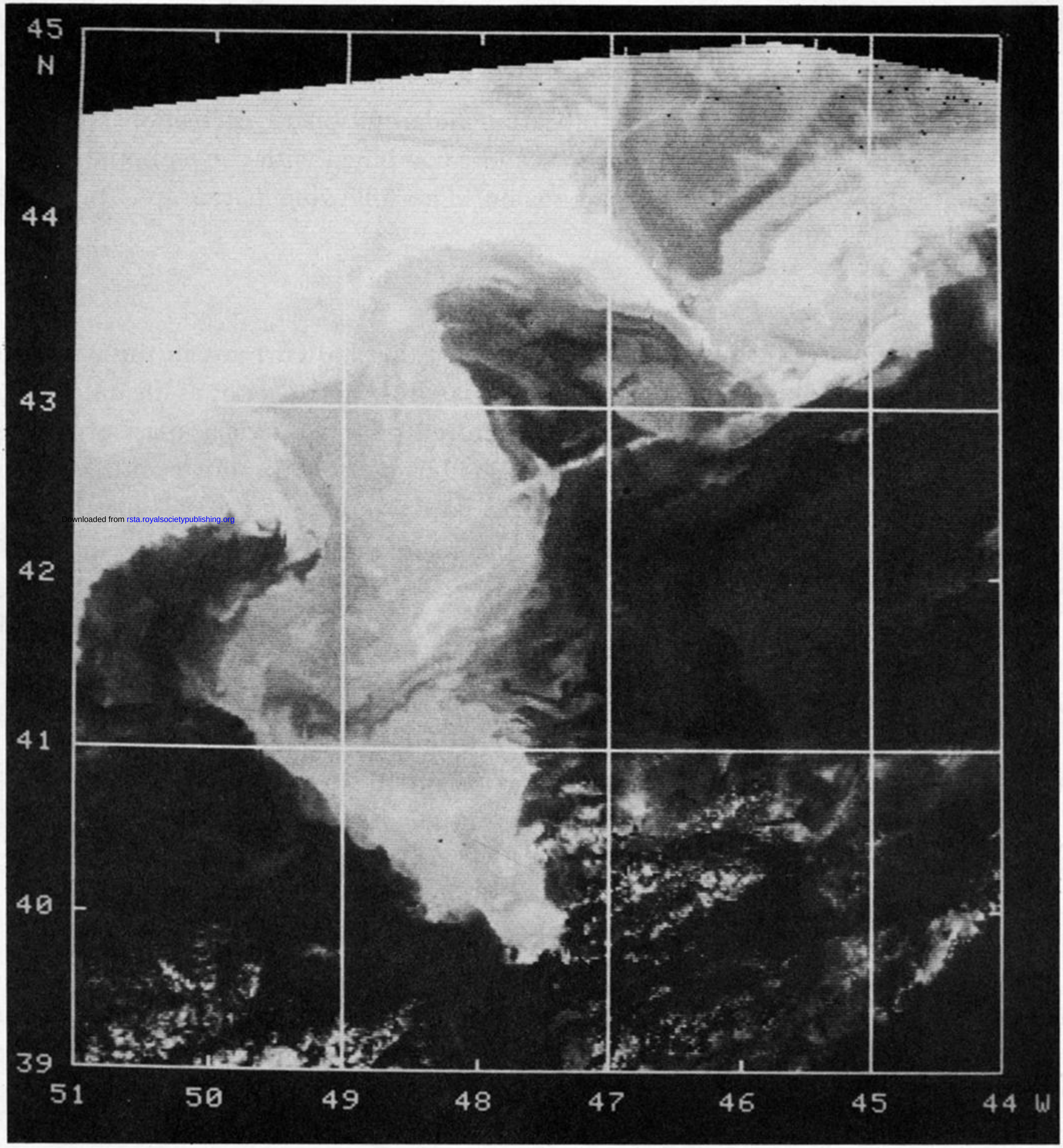

FIGURE 9. The four *TIROS-N* images in figure 6 merged into a composite designed to minimize the effect of clouds. The composite was formed by comparing the temperatures for four days at each pixel location and retaining the warmest temperature at each address for those four days (Holyer *et al.* 1980).

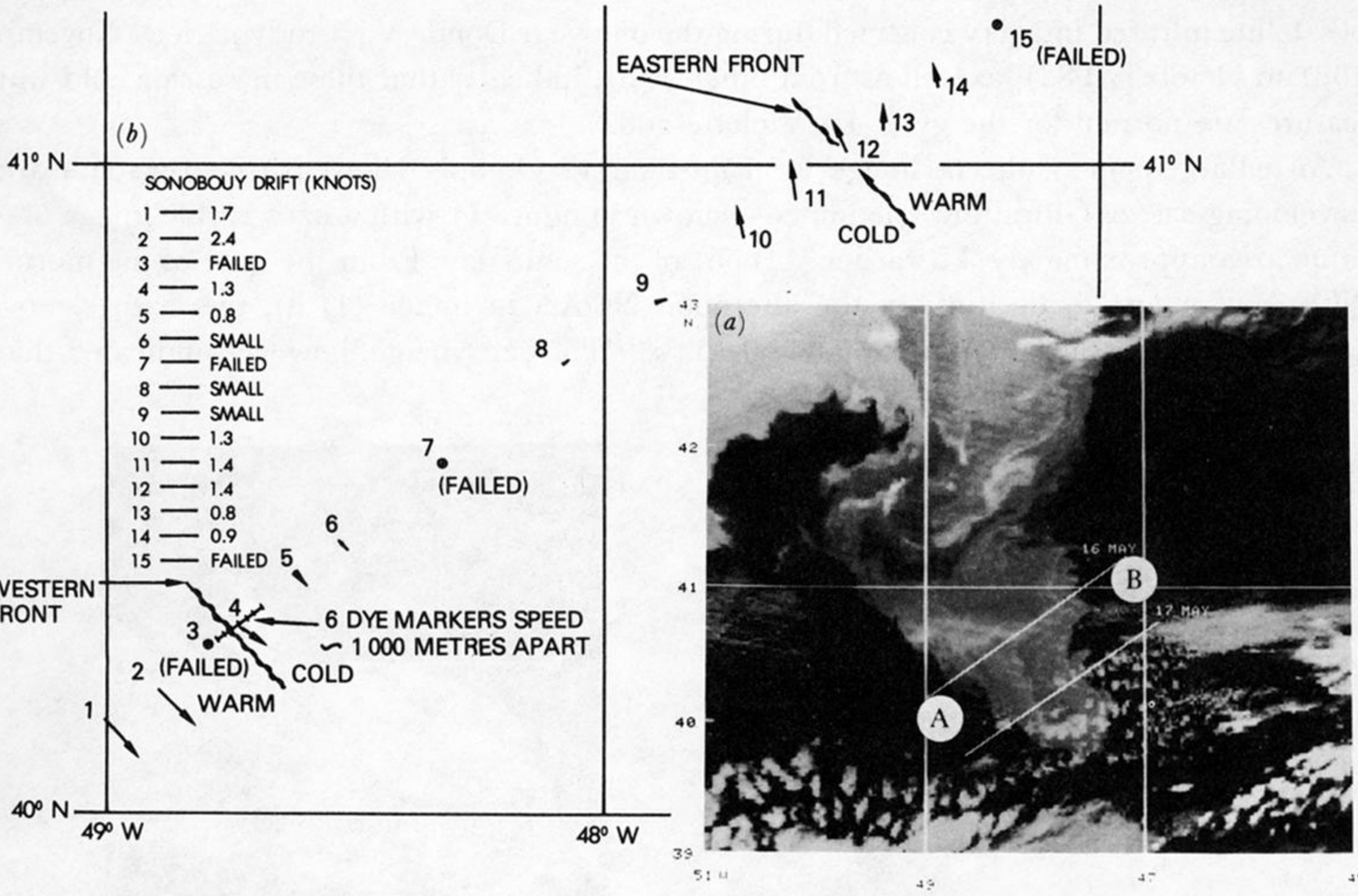

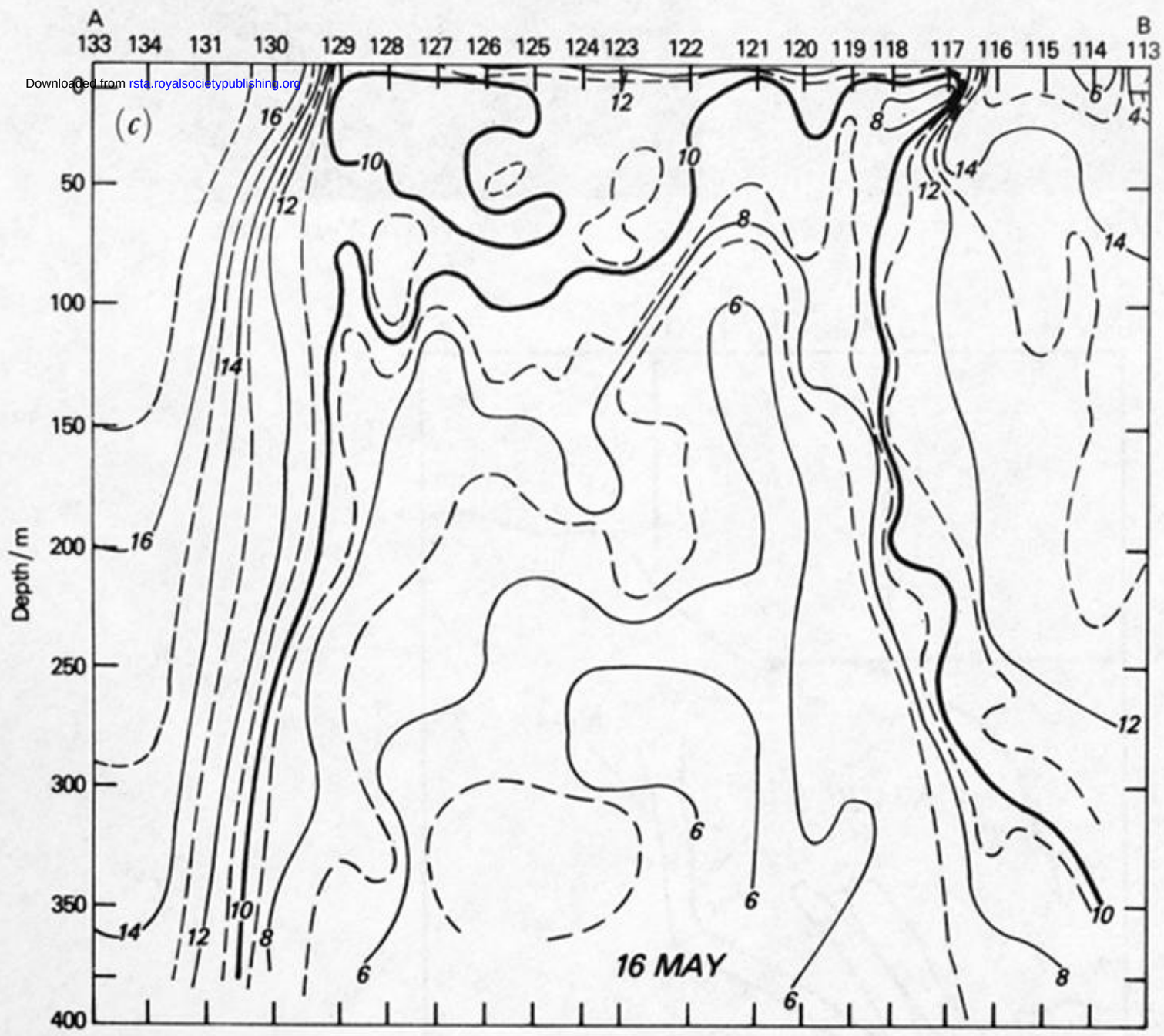

FIGURE 10. (*a*) *TIROS-N* image for 16 May 1979. Line for 16 May refers to location of sonobuoy and XBT front survey. (Lower line refers to a second airborne survey that is not shown here.) (*b*) Drift vectors based on sonobuoy data. (*c*) Temperature vertical cross section based on airborne XBT data. Numbers between A and B refer to station numbers and positions of airborne XBTS (La Violette 1983).

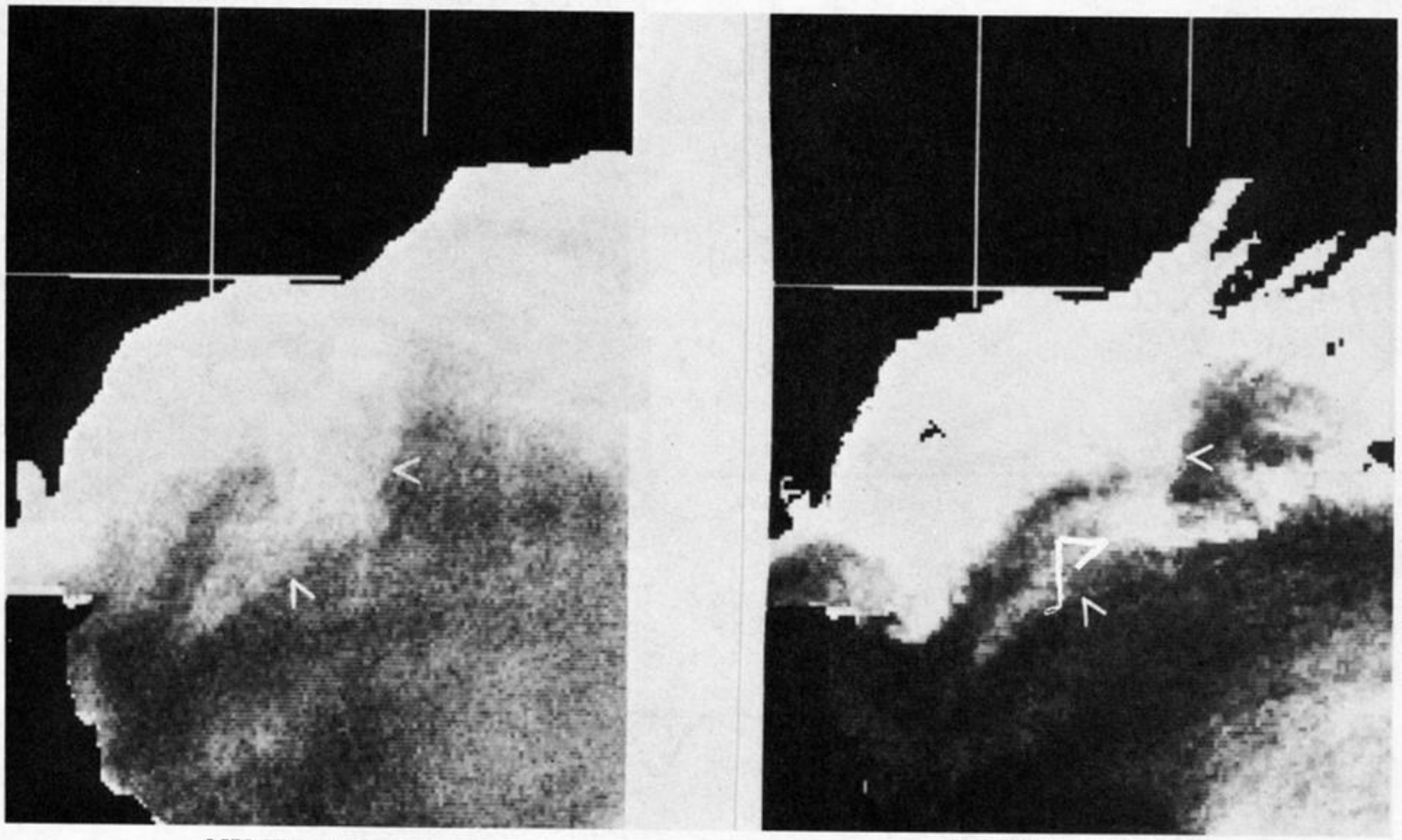

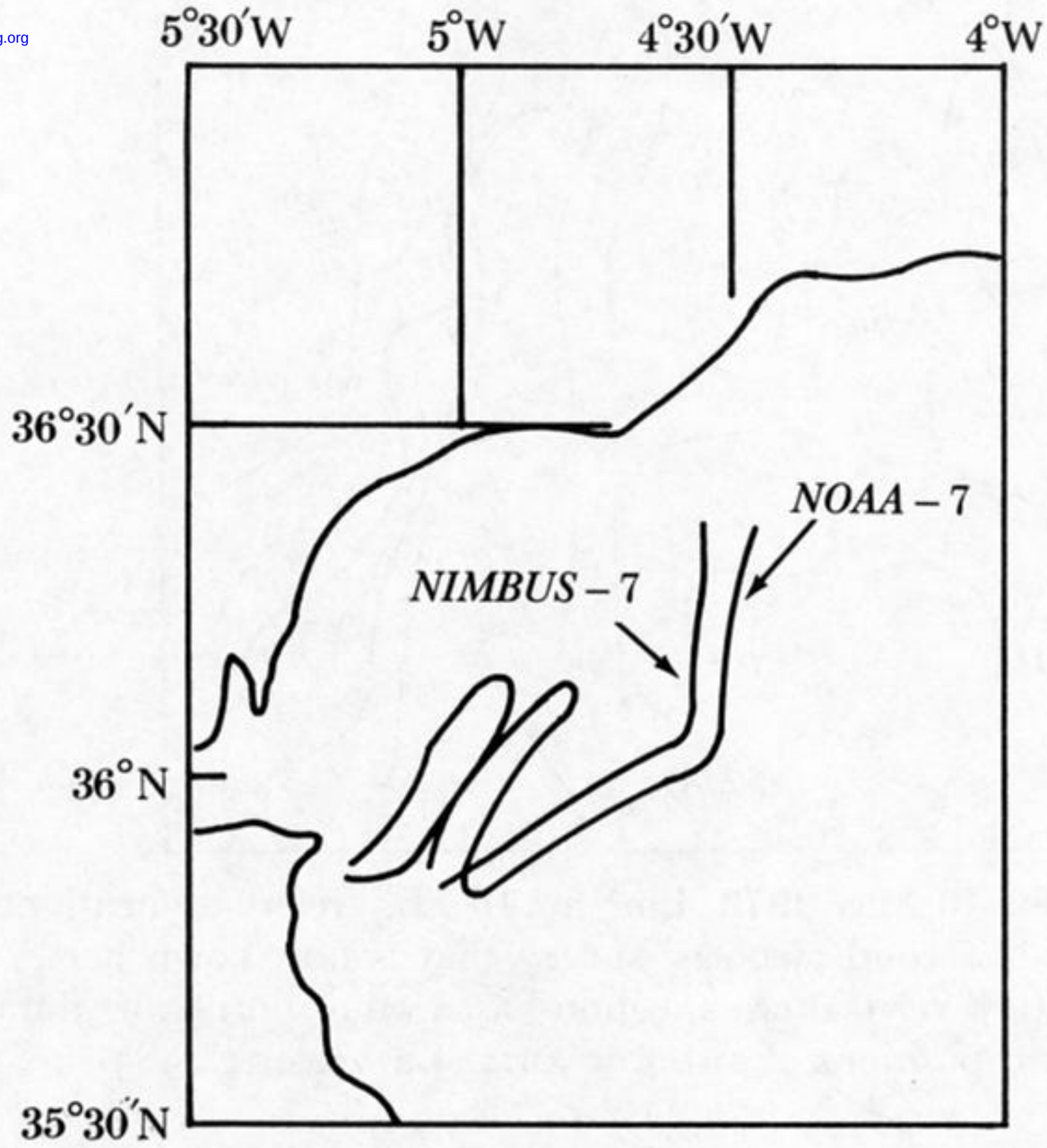

FIGURE 11. The detection of tide-current-related, short-term movement of a cold-water feature in the Alboran Sea by using Mercator-registered *Nimbus* CZCS and *NOAA*-7 AVHRR-IR imagery. The movement of approximately 9 km took place between 11h55 (*Nimbus* image) and 15h01 (NOAA image) on 12 October 1982 (La Violette 1984).